
QUANTIFYING DATASET SIMILARITY TO GUIDE TRANSFER LEARNING

A PREPRINT

Shudong Sun

Statistics and Data Science GIDP
University of Arizona
Tucson, AZ 85721
shudongsun@arizona.edu

Hao Helen Zhang

Statistics and Data Science GIDP
University of Arizona
Tucson, AZ 85721
haozhang@arizona.edu

October 28, 2025

ABSTRACT

Transfer learning has become a cornerstone of modern machine learning, as it can empower models by leveraging knowledge from related domains to improve learning effectiveness. However, transferring from poorly aligned data can harm rather than help performance, making it crucial to determine whether transfer will be beneficial before implementation. This work aims to address this challenge by proposing an innovative metric to measure dataset similarity and provide quantitative guidance on transferability. In the literature, existing methods largely focus on feature distributions while overlooking label information and predictive relationships, potentially missing critical transferability insights. In contrast, our proposed metric, the Cross-Learning Score (CLS), measures dataset similarity through bidirectional generalization performance between domains. We provide a theoretical justification for CLS by establishing its connection to the cosine similarity between the decision boundaries for the target and source datasets. Computationally, CLS is efficient and fast to compute as it bypasses the problem of expensive distribution estimation for high dimensional problems. We further introduce a general framework that categorizes source datasets into *positive*, *ambiguous*, or *negative* transfer zones based on their CLS relative to the baseline error, enabling informed decisions. Additionally, we extend this approach to encoder-head architectures in deep learning to better reflect modern transfer pipelines. Extensive experiments on diverse synthetic and real-world tasks demonstrate that CLS can reliably predict whether transfer will improve or degrade performance, offering a principled tool for guiding data selection in transfer learning.

Keywords Dataset Similarity · Transfer Learning · Transferability Measurement

1 Introduction

In machine learning and AI, knowledge transfer has become increasingly important, especially when labeled target data are scarce. For instance, a speech recognition model pre-trained on standard speech can be fine-tuned for a specific accent (Das et al., 2021; Do et al., 2024). Also, researchers may combine datasets from multiple hospitals to build a generalizable predictive model (Reps et al., 2022). In these applications, the effectiveness of knowledge transfer critically depends on similarity between the source and target data, as transfer is more beneficial for closely related tasks.

Measuring dataset similarity is a fundamental problem, as transfer learning may improve or degrade performance depending on dataset alignment. For example, Yosinski et al. (2014) demonstrated positive transfer within ImageNet, whereas Wang et al. (2019) observed negative transfer across domains in Office-31. Therefore, reliable similarity measures are essential for effective data adaptation, fine-tuning, and integration in practice of transfer learning. While the concept of dataset similarity seems intuitive, defining it rigorously remains challenging. This paper aims to introduce a new metric and establishes its theoretical foundations and empirical validity.

We focus on supervised learning, where a dataset $\mathcal{D} = \{(\mathbf{x}_i, y_i), i = 1, \dots, n\}$ is drawn from a joint distribution $\mathcal{P}(\mathbf{X}, Y)$ over $\mathcal{X} \times \mathcal{Y}$, and $\mathcal{X} \subseteq \mathbb{R}^p$ is the input space, \mathcal{Y} is the output space, n is the sample size. In transfer learning, we deal with one target dataset $\mathcal{D}^{(t)} = \{(\mathbf{x}_i^{(t)}, y_i^{(t)}), i = 1, \dots, n_t\} \sim \mathcal{P}^{(t)}$ and one source dataset $\mathcal{D}^{(s)} = \{(\mathbf{x}_i^{(s)}, y_i^{(s)}), i = 1, \dots, n_s\} \sim \mathcal{P}^{(s)}$ defined over $\mathcal{X} \times \mathcal{Y}$ but with potentially different distributions. The target dataset is typically smaller and aims to improve performance by learning from source datasets, which provide auxiliary knowledge. In multi-source transfer learning, given m source datasets $\mathcal{D}_1^{(s)}, \dots, \mathcal{D}_m^{(s)}$, the goal is to rank them by their similarity to the target dataset and integrate them via a weighting scheme that promotes positive transfer.

Various methods are proposed in literature to measure dataset similarity, such as kernel-based, divergence-based, and classification-based approaches; Stolte et al. (2023) provides a comprehensive survey. The kernel-based *Maximum Mean Discrepancy* (MMD) (Rao, 1982; Gretton et al., 2012) quantifies the distance between $\mathcal{P}^{(t)}$ and $\mathcal{P}^{(s)}$ in a Reproducing Kernel Hilbert Space. The f-divergence methods are based on the principle that two identical distributions yield identical likelihoods at every point, and quantify the deviation of the likelihood ratio from one (Zhao et al., 2022). Given any convex continuous function $f : \mathbb{R}_+ \rightarrow \mathbb{R}$ satisfying $f(1) = 0$, f-divergence is defined as

$$D_f(\mathcal{P}^{(t)} \parallel \mathcal{P}^{(s)}) = \mathbb{E}_{\mathbf{X} \sim \mathcal{P}^{(s)}} \left[f \left(\frac{p^{(t)}(\mathbf{X})}{p^{(s)}(\mathbf{X})} \right) \right],$$

where $p^{(t)}(\mathbf{x})$ and $p^{(s)}(\mathbf{x})$ denote the probability density functions of $\mathcal{P}^{(t)}$ and $\mathcal{P}^{(s)}$, respectively. Common examples include the Kullback–Leibler divergence with $f(t) = t \log t$, and the Jensen–Shannon divergence with $f(t) = (t + 1) \log(2/(t + 1)) + t \log t$.

Most of the existing methods consider only feature similarity between $\mathbf{X}^{(t)}$ and $\mathbf{X}^{(s)}$, while ignoring label information in $Y^{(t)}, Y^{(s)}$ and the feature–response relationships. This can seriously hinder transferability assessment, since datasets with similar features may represent fundamentally different prediction tasks. While label-aware methods like Optimal Transport Dataset Distance (OTDD) (Alvarez-Melis and Fusi, 2020) address this limitation, they are computationally expensive and sensitive to dimensionality.

Motivated by these limitations, we propose a new metric, **Cross-Learning Score (CLS)**, to directly quantify similarity of feature–response relationships between target and source datasets. In regression or classification, the primary objective is to learn the relationship between \mathbf{X} and Y for future prediction. When the relationships are similar across $\mathcal{D}^{(t)}$ and $\mathcal{D}^{(s)}$, both learning problems estimate the same or similar underlying function or decision boundary, making data pooling beneficial for positive transfer. When the relationships differ significantly, knowledge transfer is undermined. Based on this insight, our CLS is defined to evaluate similarity between $Y^{(t)} | \mathbf{X}^{(t)}$ and $Y^{(s)} | \mathbf{X}^{(s)}$, which is computed through bidirectional generalization performance between domains. We establish theoretical validity of CLS by proving its connection to the cosine similarity between decision boundaries for target and source datasets in some scenarios. Compared to other distance-based methods, CLS offers major computational advantages: it is efficient and scalable for high-dimensional data, bypassing the challenges of high-dimensional density estimation. We show that the robustness of CLS can be further improved through adaptive ensemble estimation.

Next, we use CLS to create a principled scheme that categorizes any source dataset into three zones based on its transferability: (1) *positive transfer* zone, where the source dataset is sufficiently similar to improve target performance; (2) *ambiguous* zone, where transfer benefits are uncertain; and (3) *negative transfer* zone, where transfer likely degrades performance. Transfer learning is fundamental to modern deep learning applications. Yang et al. (2024) survey recent deep learning approaches for similarity computation, most of which employ task-specific architectures. Finally, we extend CLS to accommodate encoder-head architectures, enabling representation-level transferability assessment aligned with current deep learning practice.

2 Cross-Learning Score (CLS)

2.1 Notations

In supervised learning, for any learner $f : \mathcal{X} \rightarrow \mathcal{Y}$, the loss function $\ell(f(\mathbf{X}), Y)$ measures the discrepancy between the predicted response given by $f(\mathbf{X})$ and the true response Y . The choice of $\ell(\cdot, \cdot)$ depends on the learning task type. For classification, the 0-1 loss $\ell(f(\mathbf{X}), Y) = \mathbb{I}[f(\mathbf{X}) \neq Y]$ measures label misclassification; for regression, the squared error loss $\ell(f(\mathbf{X}), Y) = [f(\mathbf{X}) - Y]^2$ is commonly used. The Bayes rule $f^* : \mathcal{X} \rightarrow \mathcal{Y}$ is the optimal learner that minimizes the expected loss, or risk, $R(f) = \mathbb{E}_{\mathbf{X}, Y} \ell(f(\mathbf{X}), Y)$. For regression with squared error loss, $f^*(\mathbf{X}) = \mathbb{E}[Y | \mathbf{X}]$; for classification with 0-1 loss, $f^*(\mathbf{X}) = \arg \max_y P(Y = y | \mathbf{X})$. In transfer learning, we assume the target dataset $\mathcal{D}^{(t)} \sim \mathcal{P}^{(t)}$ and source dataset $\mathcal{D}^{(s)} \sim \mathcal{P}^{(s)}$, both defined over $\mathcal{X} \times \mathcal{Y}$. Let $f^{*(t)}$ and $f^{*(s)}$ denote the Bayes rules for the target and source learning problems, respectively.

2.2 Proposed Similarity Measure

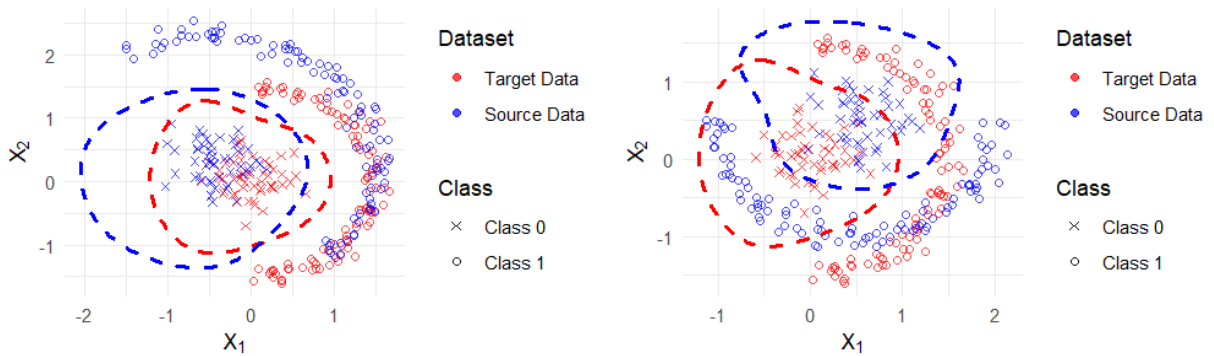
To assess similarity between target and source tasks, we consider their feature-response relationships, $Y^{(t)}|\mathbf{X}^{(t)}$ and $Y^{(s)}|\mathbf{X}^{(s)}$. Intuitively, when these relationships are similar, $f^{*(t)}$ should predict well on source data, and $f^{*(s)}$ should also predict well on target data. Figure 1 illustrates this concept with a binary classification example. Red markers indicate samples in $\mathcal{D}^{(t)}$ (“×” for class 0, “○” for class 1) with the red dashed line showing the target Bayes boundary. Blue markers indicate samples in $\mathcal{D}^{(s)}$ with the blue dashed line showing the source Bayes boundary. It is observed that, in Figure 1a, when the two Bayes boundaries are similar, both Bayes classifiers generalize well on the other dataset. In Figure 1b, when the boundaries differ substantially, each classifier trained on one task performs poorly on the other task.



(a) Linear example: similar Bayes boundaries between the target and the source data. (b) Linear example: dissimilar Bayes boundaries between the target and the source data.

Figure 1: Illustration of different feature-response relationships between the target and the source data

Figure 2 illustrates this for nonlinear classification. When the two datasets share similar decision boundaries (Figure 2a), cross-task errors are low, indicating strong similarity. When boundaries diverge (Figure 2b), high cross-task errors indicate weak similarity.



(a) Nonlinear example: similar Bayes boundaries between the target and the source data. (b) Nonlinear example: dissimilar Bayes boundaries between the target and the source data.

Figure 2: Illustration of different feature-response relationships between the target and the source data.

Motivated by the above, we introduce a new metric, the **Cross-Learning Score (CLS)**, to quantify the similarity of feature-responses relationships between the target and source tasks. In particular, CLS evaluates how well $f^{*(t)}$ predicts

on source data and $f^{*(s)}$ predicts on target data, and it is defined as their average prediction error:

$$\text{CLS} = \frac{\mathbb{E}_{(\mathbf{X}, Y) \sim \mathcal{P}^{(s)}}[\ell(f^{*(t)}(\mathbf{X}), Y)]}{2} + \frac{\mathbb{E}_{(\mathbf{X}, Y) \sim \mathcal{P}^{(t)}}[\ell(f^{*(s)}(\mathbf{X}), Y)]}{2}.$$

where $\ell(\cdot, \cdot)$ is a task-specific loss function. CLS is a positive score in $(0, 1)$ that measures average cross-task prediction performance. Lower scores indicate higher task similarity and better cross-dataset generalization, while higher scores indicate greater task divergence.

In the above formulation, both tasks are treated equally, making CLS a symmetric measure. If one task is more important than the other, a weighted average $\text{CLS}_w = w \mathbb{E}_{(\mathbf{X}, Y) \sim \mathcal{P}^{(s)}}[\ell(f^{*(t)}(\mathbf{X}), Y)] + (1 - w) \mathbb{E}_{(\mathbf{X}, Y) \sim \mathcal{P}^{(t)}}[\ell(f^{*(s)}(\mathbf{X}), Y)]$ can be used, where $0 < w < 1$ is a pre-specified weight parameter to indicate the difference.

The CLS is a theoretical concept that can not be computed without knowledge of the Bayes rule f^* . We refer to this as the *oracle* CLS. In practice, we must estimate it from data. Section 3 presents its empirical approximation, $\widehat{\text{CLS}}$, computed from the observed datasets $\mathcal{D}^{(t)}$ and $\mathcal{D}^{(s)}$ using several algorithms.

2.3 Theoretical Validity of CLS

We establish the theoretical foundation of CLS under two canonical settings, probit regression model and linear discriminant analysis (LDA). CLS is shown to be closely connected to cosine similarity between decision boundaries of the target and source tasks. Similar insight holds for nonlinear settings, but closed-form expressions are available for linear cases.

Theorem 1. Consider a binary classification problem with $\mathbf{X} \sim \mathcal{N}_p(0, I)$, and the label $Y \in \{0, 1\}$ in the target and source tasks follow the probit regression models

$$Y^{(t)} = \mathbb{I}[(\beta^{(t)\top} \mathbf{X} + \xi^{(t)}) \geq 0], Y^{(s)} = \mathbb{I}[(\beta^{(s)\top} \mathbf{X} + \xi^{(s)}) \geq 0]$$

where $\xi^{(t)}$ and $\xi^{(s)}$ are independent from $\mathcal{N}(0, \sigma^2)$. Then the Cross-Learning Score is given by

$$\text{CLS} = \frac{\arccos(\rho_1) + \arccos(\rho_2)}{2\pi},$$

$$\text{where } \rho_1 = \frac{\beta^{(t)\top} \beta^{(s)}}{\sqrt{\|\beta^{(t)}\|^2 + \sigma^2} \cdot \|\beta^{(s)}\|}, \rho_2 = \frac{\beta^{(t)\top} \beta^{(s)}}{\|\beta^{(t)}\| \cdot \sqrt{\|\beta^{(s)}\|^2 + \sigma^2}}.$$

All the proofs are provided in the Appendix. Theorem 1 shows that the CLS value is closely related to the correlation between the coefficient vectors $\beta^{(t)}$ and $\beta^{(s)}$. In the low-noise regime (σ^2 small), Lemma 1 further establishes that CLS is approximately linear in the angle between $\beta^{(t)}$ and $\beta^{(s)}$.

Lemma 1. Assume the noise variance σ^2 in Theorem 1 is sufficiently small. Then, the Cross-Learning Score between the target and source data distribution is

$$\text{CLS} \approx \frac{\theta_\beta}{\pi}, \quad \theta_\beta = \arccos\left(\frac{\beta^{(t)\top} \beta^{(s)}}{\|\beta^{(t)}\| \cdot \|\beta^{(s)}\|}\right),$$

where θ_β is the angle between $\beta^{(t)}$ and $\beta^{(s)}$.

Figure 3 illustrates the geometric interpretation of CLS when $p = 2$. A smaller angle $\theta_{\beta,1}$ (left plot) corresponds to higher task similarity and a smaller CLS value, whereas a larger angle $\theta_{\beta,2}$ (right plot) corresponds to lower similarity and a larger CLS value.

Theorem 2. Consider a Linear Discriminant Analysis (LDA) setting with balanced priors for both the target and the source data. Furthermore, assume for the target data $\mathbf{X}^{(t)}|Y^{(t)} = 1 \sim \mathcal{N}_p(\mu^{(t)}, I)$ and $\mathbf{X}^{(t)}|Y^{(t)} = 0 \sim \mathcal{N}_p(-\mu^{(t)}, I)$; for the source data, $\mathbf{X}^{(s)}|Y^{(s)} = 1 \sim \mathcal{N}_p(\mu^{(s)}, I)$ and $\mathbf{X}^{(s)}|Y^{(s)} = 0 \sim \mathcal{N}_p(-\mu^{(s)}, I)$, where $\mu^{(t)}, \mu^{(s)} \in \mathbb{R}^p$. Then

$$\text{CLS} = \frac{1}{2} \left[\Phi(-\|\mu^{(s)}\| \cos \theta_\mu) + \Phi(-\|\mu^{(t)}\| \cos \theta_\mu) \right],$$

where $\Phi(\cdot)$ is the standard Gaussian CDF and $\cos \theta_\mu = \frac{\mu^{(t)\top} \mu^{(s)}}{\|\mu^{(t)}\| \cdot \|\mu^{(s)}\|}$.

Remark. In both scenarios, CLS is theoretically linked to the cosine similarity between the target and source decision boundaries. The result aligns with the angle-based similarity metric introduced by Gu et al. (2024).

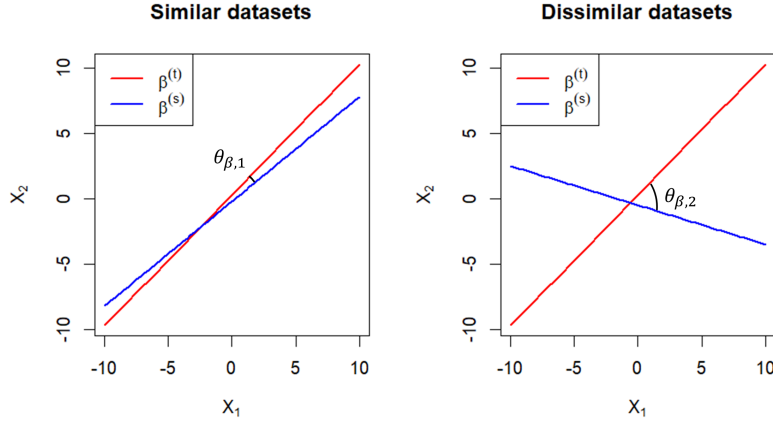


Figure 3: Illustration of target–source similarity with varying angles between $\beta^{(t)}$ and $\beta^{(s)}$ for Lemma 1

3 Computational Algorithms

Since the true Bayes rules and conditional distributions $Y^{(t)}|\mathbf{X}^{(t)}$ and $Y^{(s)}|\mathbf{X}^{(s)}$, are unknown in practice, CLS is not directly computable. We therefore develop two computational algorithms to obtain the empirical estimate $\widehat{\text{CLS}}$ from available datasets.

Algorithm 1 employs a single model M to estimate both Bayes rules: train $\hat{f}_M^{(t)}$ on $\mathcal{D}^{(t)}$ to approximate $f^{*(t)}$, and train $\hat{f}_M^{(s)}$ on $\mathcal{D}^{(s)}$ to approximate $f^{*(s)}$. The learned models are then cross-evaluated to compute average prediction losses. Details are given below.

Algorithm 1 Estimate CLS using a single model M

- 1: **Input:** Model M , target $\mathcal{D}^{(t)}$, source $\mathcal{D}^{(s)}$
- 2: Train M on $\mathcal{D}^{(t)}$ to get $\hat{f}_M^{(t)}$, then compute

$$e_M^{(t)} = \frac{1}{n_s} \sum_i \ell(\hat{f}_M^{(t)}(\mathbf{x}_i^{(s)}), y_i^{(s)})$$

- 3: Train M on $\mathcal{D}^{(s)}$ to get $\hat{f}_M^{(s)}$, then compute

$$e_M^{(s)} = \frac{1}{n_t} \sum_i \ell(\hat{f}_M^{(s)}(\mathbf{x}_i^{(t)}), y_i^{(t)})$$

- 4: **Output:** $\widehat{\text{CLS}}(M) = \frac{1}{2}(e_M^{(t)} + e_M^{(s)})$
-

The overall computational complexity of Algorithm 1 is $\mathcal{O}(C_{\text{train}}^{(t)}(M) + C_{\text{train}}^{(s)}(M))$, where $C_{\text{train}}^{(t)}(M)$ and $C_{\text{train}}^{(s)}(M)$ denote the computational cost of training M on $\mathcal{D}^{(t)}$ and $\mathcal{D}^{(s)}$, respectively. The cost of cross-domain evaluation is negligible in comparison.

The choice of model M in Algorithm 1 is important, as a poor choice may yield unreliable CLS estimates. A more robust alternative employs multiple models $\{M_1, \dots, M_l\}$, estimate the CLS value based on each model, and then aggregate their values using a weighting scheme. We discuss two such schemes below.

Scheme 1 (Weighted Average). Compute individual scores $\widehat{\text{CLS}}(M_i)$ and take their convex combination:

$$\widehat{\text{CLS}}(M_1, \dots, M_l) = \sum_{i=1}^l w_{M_i} \widehat{\text{CLS}}(M_i),$$

where $w_{M_i} \geq 0$ and $\sum_i w_{M_i} = 1$. We evaluate each model’s performance using cross-validation error and assign higher weights to better models. Specifically, we use $w_{M_i} = (w_{M_i}^{(t)} + w_{M_i}^{(s)})/2$, where the weights $w_{M_i}^{(t)}$ and $w_{M_i}^{(s)}$ given in Steps 2 and 4 of Algorithm 2.

Scheme 2 (Weighted ensemble). Instead of aggregating multiple CLS, we can ensemble predictions with dataset-specific weights obtained via cross-validation. Algorithm 2 shows details. Here $\lambda > 0$ sharpens the softmax weighting; larger λ concentrates weight on lower-CV-error models. We experimented with a range of λ values and found $\lambda = 500$ a reasonable choice.

Algorithm 2 Weighted Ensemble CLS Estimation

- 1: **Input:** Models $\{M_1, \dots, M_l\}$, datasets $\mathcal{D}^{(t)}, \mathcal{D}^{(s)}$, tuning parameter λ
- 2: Compute cross-validation error $E_{M_i}^{(t),cv}$ for each M_i on $\mathcal{D}^{(t)}$ and define

$$w_{M_i}^{(t)} = \frac{\exp(-\lambda E_{M_i}^{(t),cv})}{\sum_j \exp(-\lambda E_{M_j}^{(t),cv})}.$$

- 3: Train each M_i on $\mathcal{D}^{(t)}$, form $\hat{f}^{(t)}(x) = \sum_i w_{M_i}^{(t)} \hat{f}_{M_i}^{(t)}(x)$, then compute $e^{(t)} = \frac{1}{n_s} \sum_i \ell(\hat{f}^{(t)}(\mathbf{x}_i^{(s)}), y_i^{(s)})$.
 - 4: Repeat Steps 2–3 with roles of $\mathcal{D}^{(t)}$ and $\mathcal{D}^{(s)}$ swapped to obtain $w_{M_i}^{(s)}$ and $e^{(s)}$.
 - 5: **Output:** $\widehat{CLS}_E(M_1, \dots, M_l) = \frac{1}{2}(e^{(t)} + e^{(s)})$.
-

The computational complexity of Algorithm 2 is $\mathcal{O}\left((k+1) \sum_{i=1}^l (C_{\text{train}}^{(t)}(M_i) + C_{\text{train}}^{(s)}(M_i))\right)$, where k denotes the cross-validation folds and l the number of candidate models. The cost of inference and weight computation is negligible compared to other terms.

4 Transferable Zones

For any source dataset $\mathcal{D}^{(s)}$, after computing its CLS, we can categorize its transferability into three zones

$$\text{Zone}(\mathcal{D}^{(s)}) = \begin{cases} \text{positive transfer,} & \text{if } \widehat{CLS} < \tau_1, \\ \text{ambiguous zone,} & \text{if } \tau_1 < \widehat{CLS} < \tau_2, \\ \text{negative transfer,} & \text{if } \widehat{CLS} > \tau_2. \end{cases}$$

Here positive transfer (PT) implies high similarity and likely performance gain due to transfer; the ambiguous zone (AZ) indicates uncertain benefit; negative transfer (NT) suggests possible degrading performance (Wang and Chen, 2023). In practice, we should choose τ_1 and τ_2 carefully to ensure proper classification. We propose a systematic, data-driven approach for selecting them. Let e_0 denote the baseline test error of a model trained solely on $\mathcal{D}^{(t)}$, with $\text{SE}(e_0)$ as the standard error of its k -fold cross validation value. Define

$$\hat{\tau}_1 = e_0 + \gamma_1 \cdot \text{SE}(e_0), \quad \hat{\tau}_2 = e_0 + \gamma_2 \cdot \text{SE}(e_0),$$

where γ_1 and γ_2 control the sensitivity to negative transfer. Through extensive experiments, we find that $\gamma_1 = 1$ and $\gamma_2 = 5$ perform well across diverse examples. Their performance is presented in Section 6.

4.1 Extensions of CLS to Deep Learning

The proposed CLS is effective for shallow models (e.g., linear classifiers, SVMs), but it encounters some challenges in deep learning. One main issue is that CLS may greatly exceed the target baseline error e_0 even when transfer is beneficial. For example, when transferring from MNIST (scanned digits) to USPS (postal digits), deep models such as LeNet5 can learn rich representations from MNIST and, after fine-tuning, improve USPS accuracy. Yet, the standard CLS based on direct testing without adaptation may be much larger than $e_0 + \gamma_2 \cdot \text{SE}(e_0)$ (with $\gamma_2 = 5$), incorrectly labeling the transfer as negative. This discrepancy arises because standard CLS measures *zero-shot transferability*, i.e., performance without adaptation. Deep transfer typically follows an *encoder-head* paradigm: a shared encoder learns transferable representations, while lightweight heads adapt to domain-specific label semantics. Thus, the standard CLS underestimates transferability when joint representation learning reduces the discrepancy between domains.

To overcome this, we extend CLS to the encoder-head architecture (Algorithm 3), where a shared encoder is trained jointly on both datasets and domain-specific heads are used for cross-domain evaluation.

Algorithm 3 Estimating Encoder–Head CLS

-
- 1: **Input:** Target $\mathcal{D}^{(t)} = \{\mathcal{D}_{\text{train}}^{(t)}, \mathcal{D}_{\text{test}}^{(t)}\}$, source $\mathcal{D}^{(s)} = \{\mathcal{D}_{\text{train}}^{(s)}, \mathcal{D}_{\text{test}}^{(s)}\}$, shared encoder f_θ , heads $h^{(t)}, h^{(s)}$.
 - 2: Jointly train f_θ on $\mathcal{D}_{\text{train}}^{(t)} \cup \mathcal{D}_{\text{train}}^{(s)}$ with a temporary head (discarded after training).
 - 3: Train $h^{(s)}$ on $\mathcal{D}_{\text{train}}^{(s)}$, then compute $e^{(t)} = \frac{1}{|\mathcal{D}_{\text{test}}^{(t)}|} \sum_{(\mathbf{x}, y) \in \mathcal{D}_{\text{test}}^{(t)}} \ell(h^{(s)}(f_\theta(\mathbf{x})), y)$.
 - 4: Train $h^{(t)}$ on $\mathcal{D}_{\text{train}}^{(t)}$, then compute $e^{(s)} = \frac{1}{|\mathcal{D}_{\text{test}}^{(s)}|} \sum_{(\mathbf{x}, y) \in \mathcal{D}_{\text{test}}^{(s)}} \ell(h^{(t)}(f_\theta(\mathbf{x})), y)$.
 - 5: Compute $\widehat{\text{CLS}}_{\text{Enc-Head}} = \frac{1}{2}(e^{(t)} + e^{(s)})$.
 - 6: Compute the baseline error $e_0 = \frac{1}{|\mathcal{D}_{\text{test}}^{(t)}|} \sum_{(\mathbf{x}, y) \in \mathcal{D}_{\text{test}}^{(t)}} \ell(h^{(t)}(f_\theta(\mathbf{x})), y)$ and its standard error $\text{SE}(e_0)$.
 - 7: **Output:** $\widehat{\text{CLS}}_{\text{Enc-Head}}, e_0, \text{SE}(e_0)$
-

$\text{CLS}_{\text{Enc-Head}}$ better captures transferability in deep learning, as the encoder learns shared representations while the heads adapt to domain-specific labels. This structure aligns with practical transfer pipelines such as pretraining on $\mathcal{D}^{(s)}$ followed by fine-tuning on $\mathcal{D}^{(t)}$. When k -fold cross-validation is used to estimate $\text{SE}(e_0)$, the overall computational cost becomes $\mathcal{O}(C_{\text{enc}} + (k+1)C_{\text{head}}^{(t)} + C_{\text{head}}^{(s)})$, where C_{enc} is the encoder training cost, and $C_{\text{head}}^{(t)}, C_{\text{head}}^{(s)}$ are the costs of training the target and source heads, respectively.

5 Numerical Experiments

We conduct synthetic experiments to evaluate the effectiveness of CLS in quantifying dataset similarity for supervised learning. For binary classification, consider five settings: (i) logistic regression; (ii) probit model regression; (iii) LDA; (iv) QDA; (v) a mixture Gaussian model inducing distribution shift via a mixture parameter α . For multi-class classification, we design a four-class task where samples are projected onto two orthogonal directions and assigned to quadrants by projection signs, with Gaussian noise perturbation. For regression, we test (i) linear regression; (ii) nonlinear regression using sinusoidal, polynomial, interaction, and exponential transformations with Gaussian noise. All the details are provided in the Appendix.

For CLS estimation, we consider models for binary classification: logistic regression, linear SVM, radial SVM, XGBoost; for multi-class classification: multinomial logistic regression, linear SVM, radial SVM, XGBoost; for regression: linear regression, linear SVM, radial SVM, XGBoost. For all the experiments, we set $n_t = n_s = 200$, do 50 replicates, and report the average. Since hyperparameter tuning provided negligible performance gains but substantial cost, we present results with default configurations.

We report three CLS variants: weighted average (*Score Wtd. Avg.*), weighted ensemble (*Score Ens.*), and oracle (*Score Oracle*) which assumes knowledge of the true feature–label mapping. We compare CLS results with existing similarity measures, including KL Divergence, Wasserstein Distance, and Optimal Transport Dataset Distance (OTDD). The first two capture feature-level similarity, while OTDD accounts for label structure.

5.1 Relationships of CLS and Data Similarity

We examine the relationship between CLS and dataset similarity varies from low to high, controlled by *cosine similarity* of the model parameters in the target and source distributions or the mixing coefficient $\alpha \in [0, 1]$. See details in the Appendix.

Figure 4 shows the relationship between CLS and cosine similarity of the target and source data for binary classification settings (i)-(iii) and four-class classification. In each plot, the x-axis represents cosine similarity and the y-axis shows CLS. Three curves correspond to oracle CLS (red), weighted average estimate $\widehat{\text{CLS}}$ (green), the ensemble estimate $\widehat{\text{CLS}}_E$ (blue). Across all settings, CLS decreases monotonically as cosine similarity increases, consistent with Theorems 1 and 2, even though the data distributions are more complex. Moreover, the estimated CLS values closely approximate the oracle, indicating that both estimation schemes perform well. Results for other settings, provided in the Appendix, exhibit similar patterns.

Figure 5 compares CLS against other similarity metrics: KL Divergence, Wasserstein Distance, and Optimal Transport Dataset Distance (OTDD), as cosine similarity varies. None of them exhibits a monotonic relationship with cosine similarity under this LDA setting. Additional results are presented in the Appendix.

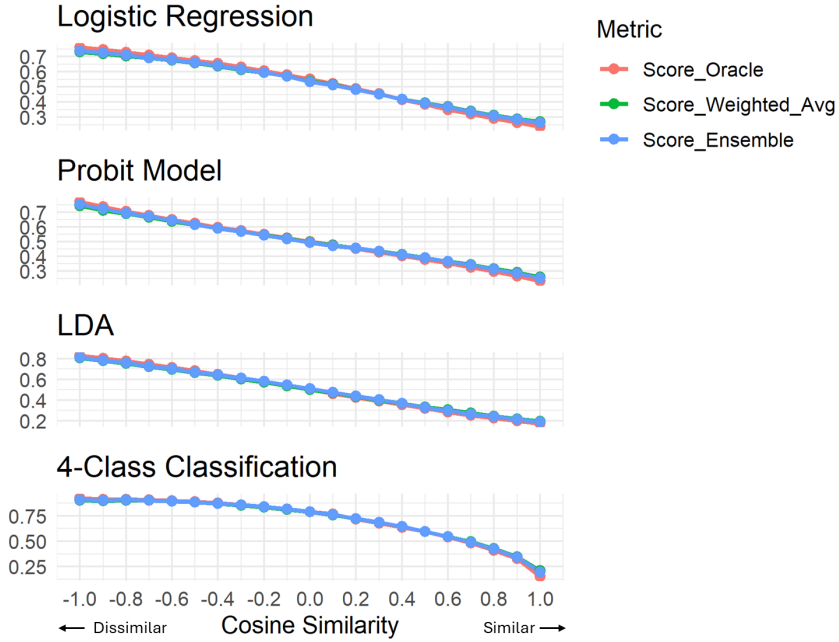


Figure 4: CLS changes with cosine similarity in several classification examples.

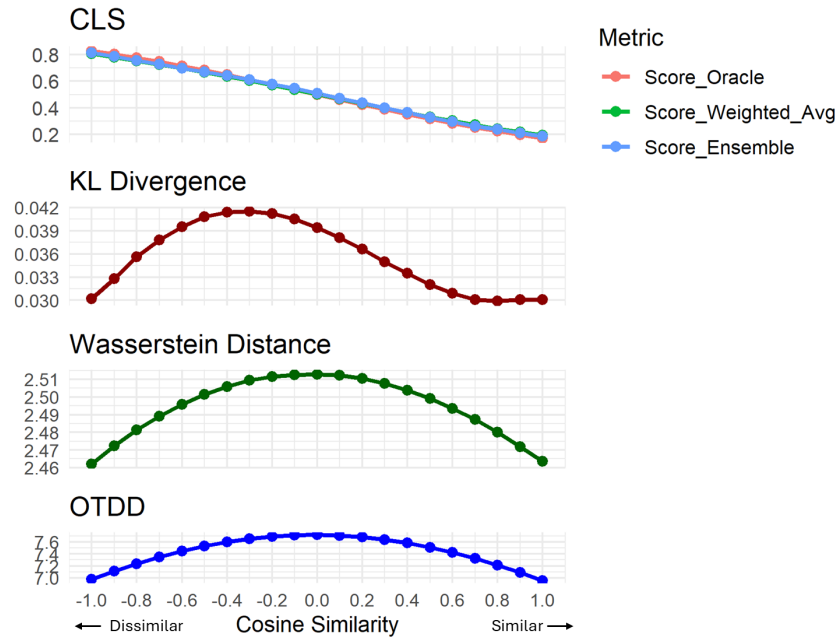


Figure 5: Comparison of CLS vs other similarity metrics under the LDA setting.

5.2 Comparison of CLS Estimation

This experiment compares different CLS estimation methods. Since the true data-generating mechanism is known, we compute the oracle CLS as the gold standard. Table 1 reports *Diff*, the average absolute deviation across all similarity

Table 1: Diff between \widehat{CLS} and oracle CLS across all the settings (Binary Classification, Multi-Class Classification, and Regression). Lower values indicate smaller deviation from the Oracle CLS.

Binary Classification								
Setting		Log.Regr.	SVM-L	SVM-R	Xgb	Unw.Avg	Wtd.Avg	Ens.
Logistic Regr.		0.0129	0.0140	0.0133	0.0321	0.0178	0.0165	0.0142
Probit		0.0063	0.0073	0.0159	0.0337	0.0157	0.0127	0.0101
LDA		0.0081	0.0084	0.0147	0.0439	0.0183	0.0147	0.0124
Mixture Gaussian		0.0109	0.0111	0.0146	0.0367	0.0175	0.0152	0.0129
QDA		0.1967	0.1957	0.1413	0.1611	0.1737	0.1685	0.1680
Multi-Class Classification								
Setting		MLR	SVM-L	SVM-R	Xgb	Unw.Avg	Wtd.Avg	Ens.
4-Class Class.		0.1694	0.2057	0.4173	0.9358	0.2154	0.1725	0.1725
Regression								
Setting		Lin.Regr.	SVM-L	SVM-R	Xgb	Unw.Avg	Wtd.Avg	Ens.
Linear Regr.		0.0942	0.0962	0.0836	0.4871	0.0957	0.0954	0.0954
Nonlinear Regr.		2.3809	2.9222	2.1255	1.3982	2.2056	1.8406	1.8299

scenarios,

$$Diff = \frac{1}{h} \sum_{i=1}^h |\widehat{CLS}_i - \text{oracle CLS}_i|,$$

where index i ranges over similarity levels from low to high. The first four columns show single-model estimates for generalized linear model, linear SVM (*SVM-L*), radial kernel SVM (*SVM-R*), and Xgb. The last three columns show multi-model estimates using three schemes: unweighted average (*Unw.Avg*), weighted average (*Wtd.Ave*), and ensemble estimate (*Ens.*).

We make several observations. Single-model performance depends heavily on alignment between model and data distributions. For linear problems (logistic regression, probit model, LDA, 4-class classification, linear regression), linear model estimates (e.g., logistic regression, SVM-Linear) achieve smaller *Diff* than nonlinear models. Conversely, for nonlinear problems (QDA, nonlinear regression), nonlinear models (SVM-Radial, XGBoost) outperform linear models. This aligns with expectations: the CLS estimation accuracy depends on how well the model fits the data. Furthermore, Among multi-model estimates, the ensemble estimate (*Ens.*) clearly outperforms the other two average, achieving the smallest *Diff* across all the settings. This suggests robustness of the ensemble estimate by integrating multiple single-model estimates, assigning higher weights to better-performing models and down-weighting poor models. We also note that the weighted average is consistently better than the unweighted average in all the settings.

5.3 Evaluation of Transferable Zones

To evaluate the proposed transferability zones, we fix the target dataset while generating the source dataset with varying similarity, controlled by cosine similarity or the mismatch parameter α . The test error of a model trained only on $\mathcal{D}^{(t)}$ is used as baseline. At each similarity level, we apply four transfer learning methods: direct concatenation (naive), TrAdaBoost Dai et al. (2007), Dynamic TrAdaBoost Al-Stouhi and Reddy (2011), Adaptive Robust Transfer Learning (ART) Wang et al. (2023), and record the number of methods outperforming the baseline.

The top panel in Figure 6 shows the average number of transfer methods (out of four) outperforming the baseline, with background colors indicating the predicted zone (PT, AZ, or NT). The bottom panel shows the difference between the test error of baseline and naive transfer. In the NT region, the curve remains flat near zero, indicating no benefit. In the AZ region, performance gradually improves; the curve typically shows an elbow. In the PT region, the curve approaches four (top panel), indicating that even naive transfer outperforms the baseline if source data is sufficiently similar.

6 Applications to Real-World Data

6.1 eICU Mortality Prediction

ICUs provide critical care for life-threatening conditions but at high cost, motivating the need for accurate post-ICU survival prediction (Halpern and Pastores, 2010, 2015; Stacy, 2011). Using the *eICU Collaborative Research Database*

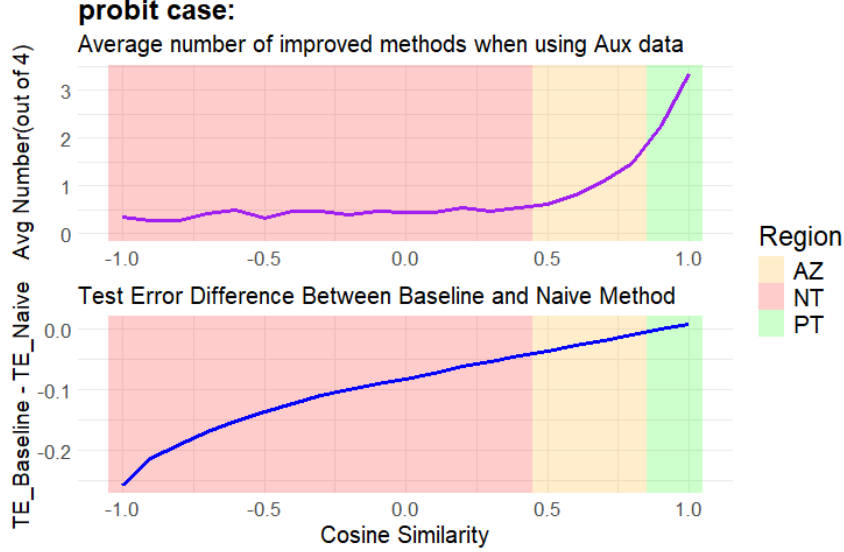


Figure 6: Transferability zones (positive, ambiguous, and negative) identified under the probit model

(Pollard et al., 2018), we construct features from demographic, hospital, and admission physiological variables after cleaning and balancing records. The hospital with the highest post-ICU mortality rate (9.47%) is used as the target, and 11 others as source datasets.

We evaluated dataset similarity using the *ensemble CLS*, based on logistic regression, linear and radial SVMs, and XGBoost, and mapped each $\mathcal{D}^{(s)}$ to a transferability zone. All 11 sources fell into the *positive transfer zone* (PT), suggesting potential transfer benefits. To validate this, we followed the experimental framework described in Wang et al. (2023). We split $\mathcal{D}^{(t)}$, consisting of 43 survivors and 43 non-survivors, into 30 training samples per class and repeated 50 times for evaluation. Random Forest achieved a baseline test error 0.408 and was adopted as the base classifier. We compared four transfer learning methods: Native (Nat), TrAdaBoost (TrA), Dynamic TrAdaBoost (DTrA), and ART across all 11 source datasets.

Table 2 reports the *relative error reduction* on the target hospital when transferring from each of the 11 source hospitals. Each value is computed as $\text{Relative Error Reduction} = \frac{e_0 - e_{\text{transfer}}}{e_0}$, where $e_0 = 0.408$ denotes the baseline test error of the target-only model, and e_{transfer} represents the test error obtained when applying a transfer learning method using a particular source dataset. A positive relative error reduction indicates that the transfer learning method improves performance (achieving a lower error), whereas a negative value indicates no improvement or performance degradation. The best-performing transfer method consistently outperformed the target-only baseline. These results align with the ensemble CLS predictions, confirming that all source datasets contributed positively to transfer learning.

6.2 Canine Image Classification

Canine image classification, particularly distinguishing dogs from wolves, offers a challenging testbed for evaluating transferability in vision tasks. Subtle inter-class differences and background confounding (e.g., snow biasing predictions toward wolves) make this task harder than standard binary classification. We use the *Roboflow Dogs vs. Wolves* dataset as $\mathcal{D}^{(t)}$ for its small size, class imbalance, and visual ambiguity. Consider three source domains with varying semantic similarity: (i) *Kaggle Dogs vs. Wolves* (1,000 per class), (ii) *Kaggle Cats vs. Dogs* (sampled 1,000 per class), and (iii) *Kaggle Horses vs. Camels* (200 per class).

We employed the *Encoder-Head CLS* (Algorithm 3) using ResNet-18 as the encoder, initialized with ImageNet weights for stable convergence. A shared encoder was jointly trained on $\mathcal{D}^{(t)}$ and $\mathcal{D}^{(s)}$, followed by domain-specific heads for cross-domain evaluation. We repeated each experiment 10 times and reported the average $\widehat{\text{CLS}}_{\text{Enc-Head}}$. Using the transferable zone prediction, *Kaggle Dogs vs Wolves* fell in the PT whereas *Kaggle Cats vs Dogs* and *Kaggle Horses vs Camels* were in the NT. For validation, the 5-fold cross-validation error on $\mathcal{D}^{(t)}$ alone served as the baseline ($e_0 = 0.0165$). To examine whether source data could improve performance, we employed a standard deep learning

Table 2: Relative error reduction on the target hospital across 11 source hospitals.

Src.	Nat	ART	TrA	DTrA	Zone
1	+0.061	+0.088	+0.015	-0.002	PT
2	+0.159	+0.125	+0.015	-0.015	PT
3	+0.076	+0.039	+0.074	+0.110	PT
4	+0.022	+0.074	-0.056	-0.064	PT
5	+0.061	+0.015	-0.066	+0.037	PT
6	+0.066	+0.098	-0.042	+0.113	PT
7	+0.081	+0.120	+0.010	+0.127	PT
8	0.000	+0.034	-0.059	+0.039	PT
9	+0.137	+0.081	-0.061	+0.039	PT
10	+0.078	+0.150	-0.074	+0.027	PT
11	+0.010	+0.010	-0.074	-0.051	PT

transfer learning setup: a ResNet-18 model was pretrained on each $\mathcal{D}^{(s)}$ (initialized from ImageNet weights) and subsequently fine-tuned on $\mathcal{D}^{(t)}$.

Table 3: Relative error reduction on Dogs vs Wolves when using transfer learning

Source Dataset	Relative Error Reduction	Zone
Dogs vs Wolves	+0.048	PT
Cats vs Dogs	-0.079	NT
Horses vs Camels	-0.091	NT

Table 3 reports the relative error reduction, computed in the same manner as in Table 2, with $e_0 = 0.0165$. We observe that the relative error reductions are **+0.048** for *Kaggle Dogs vs. Wolves*, **-0.079** for *Kaggle Cats vs. Dogs*, and **-0.091** for *Kaggle Horses vs. Camels*. Only the first source dataset yields performance gains, consistent with its Positive Transfer (PT) classification. This result confirms that the proposed CLS framework can effectively predict both beneficial and detrimental transfer in real-world vision tasks.

References

- Al-Stouhi, S. and Reddy, C. K. (2011). Adaptive boosting for transfer learning using dynamic updates. In *Joint European Conference on Machine Learning and Knowledge Discovery in Databases*, pages 60–75. Springer.
- Alvarez-Melis, D. and Fusi, N. (2020). Geometric dataset distances via optimal transport. *Advances in Neural Information Processing Systems*, 33:21428–21439.
- Dai, W., Yang, Q., Xue, G.-R., and Yu, Y. (2007). Boosting for transfer learning international conference on machine learning. In *International Conference on Machine Learning*, pages 193–200.
- Das, N., Bodapati, S., Sunkara, M., Srinivasan, S., and Chau, D. H. (2021). Best of both worlds: Robust accented speech recognition with adversarial transfer learning. *Proc. INTERSPEECH 2021*, pp. 1314–1318.
- Do, C.-T., Imai, S., Doddipatla, R., and Hain, T. (2024). Improving accented speech recognition using data augmentation based on unsupervised text-to-speech synthesis. In *2024 32nd European Signal Processing Conference (EUSIPCO)*, pages 136–140. IEEE.
- Gretton, A., Borgwardt, K. M., Rasch, M. J., Schölkopf, B., and Smola, A. (2012). A kernel two-sample test. *The Journal of Machine Learning Research*, 13(1):723–773.
- Gu, T., Han, Y., and Duan, R. (2024). Robust angle-based transfer learning in high dimensions. *Journal of the Royal Statistical Society Series B: Statistical Methodology*, page qkae111.
- Halpern, N. A. and Pastores, S. M. (2010). Critical care medicine in the united states 2000–2005: an analysis of bed numbers, occupancy rates, payer mix, and costs. *Critical care medicine*, 38(1):65–71.
- Halpern, N. A. and Pastores, S. M. (2015). Critical care medicine beds, use, occupancy, and costs in the united states: a methodological review. *Critical care medicine*, 43(11):2452–2459.
- Pardoe, D. and Stone, P. (2010). Boosting for regression transfer. In *Proceedings of the 27th International Conference on International Conference on Machine Learning*, pages 863–870.
- Pollard, T. J., Johnson, A. E., Raffa, J. D., Celi, L. A., Mark, R. G., and Badawi, O. (2018). The eicu collaborative research database, a freely available multi-center database for critical care research. *Scientific data*, 5(1):1–13.
- Rao, C. R. (1982). Diversity and dissimilarity coefficients: a unified approach. *Theoretical population biology*, 21(1):24–43.
- Reps, J. M., Williams, R. D., Schuemie, M. J., Ryan, P. B., and Rijnbeek, P. R. (2022). Learning patient-level prediction models across multiple healthcare databases: evaluation of ensembles for increasing model transportability. *BMC medical informatics and decision making*, 22(1):142.
- Stacy, K. M. (2011). Progressive care units: different but the same. *Critical Care Nurse*, 31(3):77–83.
- Stolte, M., Bommert, A., and Rahnenführer, J. (2023). A review and taxonomy of methods for quantifying dataset similarity. *arXiv preprint arXiv:2312.04078*.
- Wang, B., Wu, Y., and Ye, C. (2023). The art of transfer learning: An adaptive and robust pipeline. *Stat*, 12(1):e582.
- Wang, J. and Chen, Y. (2023). *Introduction to transfer learning: algorithms and practice*. Springer Nature.
- Wang, Z., Dai, Z., Póczos, B., and Carbonell, J. (2019). Characterizing and avoiding negative transfer. In *Proceedings of the IEEE/CVF conference on computer vision and pattern recognition*, pages 11293–11302.
- Yang, P., Wang, H., Yang, J., Qian, Z., Zhang, Y., and Lin, X. (2024). Deep learning approaches for similarity computation: A survey. *IEEE Transactions on Knowledge and Data Engineering*, 36(12):7893–7912.
- Yosinski, J., Clune, J., Bengio, Y., and Lipson, H. (2014). How transferable are features in deep neural networks? *Advances in neural information processing systems*, 27.
- Zhang, W., Zhong, M., Tandon, R., and Krunz, M. (2024). Filtered randomized smoothing: A new defense for robust modulation classification. In *MILCOM 2024-2024 IEEE Military Communications Conference (MILCOM)*, pages 789–794. IEEE.
- Zhao, S., Sinha, A., He, Y., Perreault, A., Song, J., and Ermon, S. (2022). Comparing distributions by measuring differences that affect decision making. In *International Conference on Learning Representations*.
- Zhong, M. and Tandon, R. (2023). Learning fair classifiers via min-max f-divergence regularization. In *2023 59th Annual Allerton Conference on Communication, Control, and Computing (Allerton)*, pages 1–8. IEEE.
- Zhong, M. and Tandon, R. (2024a). Intrinsic fairness-accuracy tradeoffs under equalized odds. In *2024 IEEE International Symposium on Information Theory (ISIT)*, pages 220–225. IEEE.

- Zhong, M. and Tandon, R. (2024b). Learning fair robustness via domain mixup. In *2024 58th Asilomar Conference on Signals, Systems, and Computers*, pages 196–202. IEEE.
- Zhong, M. and Tandon, R. (2025). Splitz: Certifiable robustness via split lipschitz randomized smoothing. *IEEE Transactions on Information Forensics and Security*.

A ADDITIONAL MATERIAL FOR SECTION 2

This section contains the proofs of the results presented in Section 2.

A.1 Proof of Theorem 1

Proof. For the target learning problem, the Bayes rule is given by:

$$f^{*(t)}(\mathbf{X}) = \begin{cases} 1, & \text{if } (\beta^{(t)\top} \mathbf{X} + \xi) \geq 0, \\ 0, & \text{if } (\beta^{(t)\top} \mathbf{X} + \xi) < 0. \end{cases}$$

The classification error when applying the target classifier to the source data, denoted as $e^{(t)}$, represents the first half of the CLS. :

$$\begin{aligned} e^{(t)} &= \mathbb{E}_{(\mathbf{X}^{(s)}, Y^{(s)}) \sim \mathcal{P}^{(s)}} \left[\ell(f^{*(t)}(\mathbf{X}^{(s)}), Y^{(s)}) \right] \\ &= \mathbb{E} \left[\mathbb{I}(f^{*(t)}(\mathbf{X}^{(s)}) \neq Y^{(s)}) \right] \\ &= \mathbb{P}(f^{*(t)}(\mathbf{X}^{(s)}) \neq Y^{(s)}) \\ &= \mathbb{P}(f^{*(t)}(\mathbf{X}^{(s)}) = 1, Y^{(s)} = 0) + \mathbb{P}(f^{*(t)}(\mathbf{X}^{(s)}) = 0, Y^{(s)} = 1) \\ &= \mathbb{P}[\beta^{(t)\top} \mathbf{X}^{(s)} + \xi \geq 0, \beta^{(s)\top} \mathbf{X}^{(s)} < 0] + \mathbb{P}[\beta^{(t)\top} \mathbf{X}^{(s)} + \xi < 0, \beta^{(s)\top} \mathbf{X}^{(s)} \geq 0]. \end{aligned}$$

Since $\mathbf{X}^{(s)}$ follows an i.i.d. normal distribution:

$$\mathbf{X}^{(s)} \sim \mathcal{N}_p(0, I),$$

the linear projections $\beta^{(s)\top} \mathbf{X}^{(s)}$ and $\beta^{(t)\top} \mathbf{X}^{(s)}$ are also normally distributed:

$$\beta^{(t)\top} \mathbf{X}^{(s)} + \xi \sim \mathcal{N}(0, \beta^{(t)\top} \beta^{(t)} + \sigma^2), \quad \beta^{(s)\top} \mathbf{X}^{(s)} \sim \mathcal{N}(0, \beta^{(s)\top} \beta^{(s)}).$$

The covariance between these projections is given by:

$$\text{cov}(\beta^{(t)\top} \mathbf{X} + \xi, \beta^{(s)\top} \mathbf{X}) = \text{cov}(\beta^{(t)\top} \mathbf{X}, \beta^{(s)\top} \mathbf{X}) = \beta^{(t)\top} \beta^{(s)}.$$

Thus, the joint covariance matrix is:

$$\Sigma_{\text{joint}} = \begin{pmatrix} \beta^{(t)\top} \beta^{(t)} + \sigma^2 & \beta^{(t)\top} \beta^{(s)} \\ \beta^{(t)\top} \beta^{(s)} & \beta^{(s)\top} \beta^{(s)} \end{pmatrix}.$$

To obtain standard normal variables, we define:

$$Z_t = \frac{\beta^{(t)\top} \mathbf{X}^{(s)} + \xi}{\sqrt{\beta^{(t)\top} \beta^{(t)} + \sigma^2}} \sim \mathcal{N}(0, 1), \quad Z_s = \frac{\beta^{(s)\top} \mathbf{X}^{(s)}}{\sqrt{\beta^{(s)\top} \beta^{(s)}}} \sim \mathcal{N}(0, 1).$$

The joint distribution of (Z_t, Z_s) is a bivariate normal with zero mean and covariance matrix:

$$\Sigma_Z = \begin{pmatrix} 1 & \rho_1 \\ \rho_1 & 1 \end{pmatrix}.$$

where

$$\rho_1 = \frac{\beta^{(t)\top} \beta^{(s)}}{\sqrt{\beta^{(t)\top} \beta^{(t)} + \sigma^2} \sqrt{\beta^{(s)\top} \beta^{(s)}}}.$$

Its density is given by:

$$f(z_t, z_s) = \frac{1}{2\pi\sqrt{1-\rho_1^2}} \exp\left(-\frac{z_t^2 - 2\rho_1 z_t z_s + z_s^2}{2(1-\rho_1^2)}\right).$$

The classification error corresponds to the probability that $Z_t \geq 0$ and $Z_s < 0$ (or vice versa):

$$\mathbb{P}(Z_t \geq 0, Z_s < 0) = \int_0^\infty \int_{-\infty}^0 f(z_t, z_s) dz_s dz_t.$$

A known result from bivariate normal probability computations states:

$$\mathbb{P}(Z_t \geq 0, Z_s < 0) = \frac{\arccos(\rho_1)}{2\pi}.$$

Since $\mathbb{P}(Z_t < 0, Z_s \geq 0)$ is symmetric, we obtain:

$$e^{(t)} = \mathbb{P}(Z_t \geq 0, Z_s < 0) + \mathbb{P}(Z_t < 0, Z_s \geq 0) = \frac{\arccos(\rho_1)}{\pi}.$$

Thus, the classification error when applying the target classifier to the source data is:

$$e^{(t)} = \frac{\arccos(\rho_1)}{\pi}.$$

Similarly, the classification error when applying the source classifier to the target data is:

$$e^{(s)} = \frac{\arccos(\rho_2)}{\pi}.$$

where

$$\rho_2 = \frac{\beta^{(t)\top} \beta^{(s)}}{\sqrt{\beta^{(t)\top} \beta^{(t)}} \sqrt{\beta^{(s)\top} \beta^{(s)} + \sigma^2}}.$$

Then

$$\text{CLS} = \frac{e^{(t)} + e^{(s)}}{2} = \frac{\arccos(\rho_1) + \arccos(\rho_2)}{2\pi}.$$

where

$$\rho_1 = \frac{\beta^{(t)\top} \beta^{(s)}}{\sqrt{\beta^{(t)\top} \beta^{(t)} + \sigma^2} \sqrt{\beta^{(s)\top} \beta^{(s)}}}, \quad \rho_2 = \frac{\beta^{(t)\top} \beta^{(s)}}{\sqrt{\beta^{(t)\top} \beta^{(t)}} \sqrt{\beta^{(s)\top} \beta^{(s)} + \sigma^2}}.$$

□

A.2 Proof of Lemma 1

Proof. When σ^2 is sufficiently small, the correlation coefficient simplifies to:

$$\rho_1 \approx \rho_2 \approx \rho = \frac{\beta^{(t)\top} \beta^{(s)}}{\|\beta^{(t)}\| \cdot \|\beta^{(s)}\|} = \cos \theta_\beta,$$

where θ is the angle between $\beta^{(t)}$ and $\beta^{(s)}$.

Then

$$e^{(t)} = e^{(s)} \approx \frac{\arccos(\rho)}{\pi} = \frac{\theta_\beta}{\pi}.$$

The CLS is given by:

$$\text{CLS} = \frac{e^{(t)} + e^{(s)}}{2} \approx \frac{\theta_\beta}{\pi}.$$

where

$$\theta_\beta = \arccos\left(\frac{\beta^{(t)\top} \beta^{(s)}}{\|\beta^{(t)}\| \cdot \|\beta^{(s)}\|}\right).$$

□

A.3 Proof of Theorem 2

Proof. Consider a simple Linear Discriminant Analysis (LDA) setting. We assume that the target data follows the distributions:

$$\mathbf{X}^{(t)} | Y^{(t)} = 1 \sim \mathcal{N}_p(\mu^{(t)}, I), \quad \mathbf{X}^{(t)} | Y^{(t)} = 0 \sim \mathcal{N}_p(-\mu^{(t)}, I),$$

and the source data follows:

$$\mathbf{X}^{(s)} | Y^{(s)} = 1 \sim \mathcal{N}_p(\mu^{(s)}, I), \quad \mathbf{X}^{(s)} | Y^{(s)} = 0 \sim \mathcal{N}_p(-\mu^{(s)}, I),$$

where both $\mu^{(t)}$ and $\mu^{(s)}$ are p -dimensional vectors. The class priors are assumed to be balanced:

$$P(Y^{(t)} = 1) = P(Y^{(t)} = 0) = \frac{1}{2}, \quad P(Y^{(s)} = 1) = P(Y^{(s)} = 0) = \frac{1}{2}.$$

The probability density functions (PDFs) for the target data are given by:

$$p(\mathbf{X}^{(t)} | Y^{(t)} = 1) = \frac{1}{(2\pi)^{p/2}} \exp\left(-\frac{1}{2}(\mathbf{X}^{(t)} - \mu^{(t)})^\top (\mathbf{X}^{(t)} - \mu^{(t)})\right),$$

$$p(\mathbf{X}^{(t)} | Y^{(t)} = 0) = \frac{1}{(2\pi)^{p/2}} \exp\left(-\frac{1}{2}(\mathbf{X}^{(t)} + \mu^{(t)})^\top (\mathbf{X}^{(t)} + \mu^{(t)})\right).$$

The Bayesian classification rule assigns $\mathbf{X}^{(t)}$ to class $Y^{(t)} = 1$ if:

$$p(\mathbf{X}^{(t)} | Y^{(t)} = 1) > p(\mathbf{X}^{(t)} | Y^{(t)} = 0).$$

Taking the natural logarithm on both sides and substituting the Gaussian PDFs, we obtain:

$$-\frac{1}{2}(\mathbf{X}^{(t)} - \mu^{(t)})^\top (\mathbf{X}^{(t)} - \mu^{(t)}) > -\frac{1}{2}(\mathbf{X}^{(t)} + \mu^{(t)})^\top (\mathbf{X}^{(t)} + \mu^{(t)}).$$

Expanding and simplifying, we derive the classification rule:

$$\mu^{(t)\top} \mathbf{X}^{(t)} > 0.$$

Thus, the Bayesian decision boundary for the target data is given by:

$$\mu^{(t)\top} \mathbf{X}^{(t)} = 0.$$

The Bayes rule for the target learning problem is then defined as:

$$f^{*(t)}(\mathbf{X}) = \begin{cases} 1, & \text{if } \mu^{(t)\top} \mathbf{X} \geq 0, \\ 0, & \text{if } \mu^{(t)\top} \mathbf{X} < 0. \end{cases}$$

The classification error when applying the target classifier to the source data, denoted as $e^{(t)}$, represents the first half of the CLS:

$$\begin{aligned} e^{(t)} &= \mathbb{E}_{(\mathbf{X}^{(s)}, Y^{(s)}) \sim \mathcal{P}^{(s)}} \left[\ell(f^{*(t)}(\mathbf{X}^{(s)}), Y^{(s)}) \right] \\ &= \mathbb{E} \left[\mathbb{I}(f^{*(t)}(\mathbf{X}^{(s)}) \neq Y^{(s)}) \right] \\ &= \mathbb{P}(f^{*(t)}(\mathbf{X}^{(s)}) \neq Y^{(s)}) \\ &= \mathbb{P}(f^{*(t)}(\mathbf{X}^{(s)}) = 1, Y^{(s)} = 0) + \mathbb{P}(f^{*(t)}(\mathbf{X}^{(s)}) = 0, Y^{(s)} = 1) \\ &= \mathbb{P}(f^{*(t)}(\mathbf{X}^{(s)}) = 1 | Y^{(s)} = 0) \cdot \mathbb{P}(Y^{(s)} = 0) + \mathbb{P}(f^{*(t)}(\mathbf{X}^{(s)}) = 0 | Y^{(s)} = 1) \cdot \mathbb{P}(Y^{(s)} = 1) \\ &= \frac{1}{2} \mathbb{P}(\mu^{(t)\top} \mathbf{X}^{(s)} \geq 0 | Y^{(s)} = 0) + \frac{1}{2} \mathbb{P}(\mu^{(t)\top} \mathbf{X}^{(s)} < 0 | Y^{(s)} = 1). \end{aligned}$$

Given:

$$\mathbf{X}^{(s)} | Y^{(s)} = 0 \sim \mathcal{N}_p(-\mu^{(s)}, I), \quad \mathbf{X}^{(s)} | Y^{(s)} = 1 \sim \mathcal{N}_p(\mu^{(s)}, I),$$

we know that:

$$\mu^{(t)\top} \mathbf{X}^{(s)} \mid Y^{(s)} = 0 \sim \mathcal{N}(-\mu^{(t)\top} \mu^{(s)}, \|\mu^{(t)}\|^2). \quad \mu^{(t)\top} \mathbf{X}^{(s)} \mid Y^{(s)} = 1 \sim \mathcal{N}(\mu^{(t)\top} \mu^{(s)}, \|\mu^{(t)}\|^2),$$

Thus, the error becomes:

$$e^{(t)} = \frac{1}{2} \Phi \left(\frac{-\mu^{(t)\top} \mu^{(s)}}{\|\mu^{(t)}\|} \right) + \frac{1}{2} \left[1 - \Phi \left(\frac{\mu^{(t)\top} \mu^{(s)}}{\|\mu^{(t)}\|} \right) \right] = \Phi \left(\frac{-\mu^{(t)\top} \mu^{(s)}}{\|\mu^{(t)}\|} \right) = \Phi(-\|\mu^{(s)}\| \cos \theta_\mu),$$

where

$$\cos \theta_\mu = \frac{\mu^{(t)\top} \mu^{(s)}}{\|\mu^{(t)}\| \|\mu^{(s)}\|}$$

is the cosine similarity between $\mu^{(t)}$ and $\mu^{(s)}$, and $\Phi(\cdot)$ is the standard Gaussian CDF.

Similarly, the Bayesian decision boundary for the source data is:

$$\mu^{(s)\top} \mathbf{X}^{(s)} = 0.$$

The Bayes rule for the source learning problem is then defined as:

$$f^{*(s)}(\mathbf{X}) = \begin{cases} 1, & \text{if } \mu^{(s)\top} \mathbf{X} \geq 0, \\ 0, & \text{if } \mu^{(s)\top} \mathbf{X} < 0. \end{cases}$$

Following the same reasoning as before, the misclassification probability when using $f^{*(s)}$ on the target data is:

$$e^{(s)} = \Phi(-\|\mu^{(t)}\| \cos \theta_\mu).$$

The CLS is then computed as:

$$\text{CLS} = \frac{e^{(t)} + e^{(s)}}{2} = \frac{\Phi(-\|\mu^{(s)}\| \cos \theta_\mu) + \Phi(-\|\mu^{(t)}\| \cos \theta_\mu)}{2}.$$

□

B ADDITIONAL MATERIAL FOR SECTION 5

In this section, we present the detailed setup of the synthetic experiments designed to evaluate the effectiveness of CLS in quantifying dataset similarity for supervised learning.

Let $\nu^{(t)}$ denote the parameter vector for the target data and $\nu^{(s)}$ denote that for the source data. Given $\nu^{(t)}$, Section B.1 introduces a method to generate $\nu^{(s)}$ with controlled cosine similarity to $\nu^{(t)}$.

We design eight distinct experimental settings to characterize the similarity between target and source data, using the generation method described in Section B.1. The details and results for these settings are presented in Sections B.2–B.4. For all experiments, we set $n_t = n_s = 200$, conduct 50 independent replicates, and report the averaged results. To assess prediction accuracy, an additional 5,000 data points are independently generated as the test set.

Each setting contains two figures and two tables, which are described in the following four paragraphs.

The first figure (Figure 8, 10, 12, 14, 16, 18, 20, 22) in each setting illustrates the relationship between the estimated similarity metrics and the underlying data similarity, which is controlled either by the cosine similarity between the model parameters of the target and source distributions or by the mixing coefficient $\alpha \in [0, 1]$. In each plot, the x-axis represents data similarity, while the y-axis shows various similarity metrics, including three variants of the CLS: the oracle CLS (red), the weighted-average estimate $\widehat{\text{CLS}}$ (light green), and the ensemble estimate $\widehat{\text{CLS}}_E$ (light blue), as well as benchmark measures such as KL Divergence (brown), Wasserstein Distance (dark green), and Optimal Transport Dataset Distance (OTDD) (dark blue).

The second figure (Figure 9, 11, 13, 15, 17, 19, 21, 23) in each setting presents the evaluation results for the proposed transferable zones. The top panel shows the average number of transfer methods outperforming the baseline, with background colors indicating the predicted zone (PT, AZ, or NT). The bottom panel shows the difference between the test error of the baseline and the naive transfer method.

The first table (Table 4, 6, 8, 10, 12, 14, 16, 18) in each setting presents comparisons of various similarity score metrics across different cosine similarity values or mixture parameters α in the mixture Gaussian setting. For each configuration, we additionally report the corresponding KL Divergence, Wasserstein Distance, and Optimal Transport Dataset Distance (OTDD) metrics (noting that OTDD cannot be directly computed for regression tasks). The notation $|\rho_p|$ denotes the absolute value of the Pearson correlation coefficient between each metric and the cosine similarity, while $|\rho_s|$ represents the absolute value of the Spearman rank correlation coefficient. Mathematically, the Pearson and Spearman correlation coefficients between KL Divergence or Wasserstein Distance and cosine similarity are undefined; for convenience, we set them to zero in our analysis.

The second table (Table 5, 7, 9, 11, 13, 15, 17, 19) in each setting present comparisons of various estimated CLS values across different cosine similarity levels or mixture parameters α in the mixture Gaussian setting. *Diff.* denotes the mean absolute difference between each estimated score and the oracle CLS, as defined in Section 5.2. Lower values indicate smaller deviation from the Oracle CLS. The first column reports the optimal-model estimates assuming access to the Bayes rule of the target learning problem. The next four columns show single-model estimates obtained from the generalized linear model, linear SVM, radial SVM, and XGBoost. The following three columns present multi-model estimates based on unweighted average (*Unw.Avg.*), weighted average (*Wtd.Avg.*), and ensemble (*Ens.*) schemes using the above four single models. The final column lists the Oracle CLS as the reference gold standard.

The correspondence between each setting and its associated figures and tables will be presented later.

B.1 Generating Source Parameter Vectors with Controlled Cosine Similarity

We begin by considering the parameter vectors $\nu^{(t)}$ corresponding to the target data. The source parameter vectors $\nu^{(s)}$ are then generated using the procedure described below to control the cosine similarity between $\nu^{(t)}$ and $\nu^{(s)}$.

To illustrate the process of generating $\nu^{(s)}$, we begin with a three-dimensional space ($p = 3$) by transforming the Cartesian coordinates $\nu^{(t)} = (x_t, y_t, z_t)$ into spherical coordinates (r, θ_t, ϕ) using the following equations:

$$\begin{aligned} r &= \sqrt{x_t^2 + y_t^2 + z_t^2} \\ \theta_t &= \arccos\left(\frac{z_t}{r}\right) \\ \phi &= \arccos\left(\frac{x_t}{r \cdot \sin \theta_t}\right) \end{aligned}$$

In these equations, the radius r indicates the Euclidean distance from the origin to the point, the polar angle θ_t quantifies the angle between the positive z -axis and the point, and the azimuthal angle ϕ measures the angle between the positive x -axis and the projection of the point onto the xy -plane.

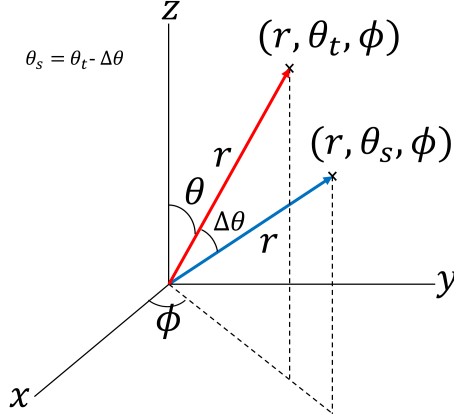


Figure 7: illustration to generate the new vector $\nu^{(s)}$

To generate a new vector $\nu^{(s)}$ for source data, we maintain a constant azimuthal angle ϕ and modify the polar angle θ_t to θ_s . The detailed steps are as follows:

1. *Defining Cosine Similarity Values:* Begin by defining a set of cosine similarity values, denoted by t , which are uniformly distributed between -1 and 1. These values correspond to the desired similarity relative to the original vector's orientation for target data.
2. *Determining Angular Shifts:* Using the cosine similarity values, calculate the corresponding changes in the polar angle, $\Delta\theta$, by taking the inverse cosine (arccos) of the similarity values: $\Delta\theta = \arccos(t)$. This calculation establishes the angular adjustments necessary to reach the specified similarities.
3. *Computing New Polar Angles:* Derive the new polar angles, θ_s , by subtracting the angular shifts, $\Delta\theta$, from the original polar angle, θ_t : $\theta_s = \theta_t - \Delta\theta$. This operation results in a series of modified polar angles while retaining the original the radius r and azimuthal angle ϕ .
4. *Reconstructing Cartesian Coordinates:* Finally, utilize the updated polar angles θ_s and the unchanged r , ϕ to convert back to Cartesian coordinates, thereby defining the new vector $\nu^{(s)} = (x_s, y_s, z_s)$. The updated coordinates are given by:

$$\begin{aligned} x_s &= r \sin \theta_s \cos \phi \\ y_s &= r \sin \theta_s \sin \phi \\ z_s &= r \cos \theta_s \end{aligned}$$

This systematic approach facilitates the controlled generation of a new vector $\nu^{(s)}$ by varying the polar angle θ while preserving the orientation in the xy -plane. This method is especially useful for applications that demand precise directional control.

Let us calculate the cosine similarity between $\nu^{(t)}$ and $\nu^{(s)}$, denoted as $S_C(\nu^{(t)}, \nu^{(s)})$:

$$\begin{aligned} S_C(\nu^{(t)}, \nu^{(s)}) &= \frac{\nu^{(t)} \cdot \nu^{(s)}}{\|\nu^{(t)}\| \|\nu^{(s)}\|} = \frac{x_t \cdot x_s + y_t \cdot y_s + z_t \cdot z_s}{\sqrt{x_t^2 + y_t^2 + z_t^2} \sqrt{x_s^2 + y_s^2 + z_s^2}} \\ &= \frac{r \cdot \sin \theta_t \cdot \cos \phi \cdot r \cdot \sin \theta_s \cdot \cos \phi + r \cdot \sin \theta_t \cdot \sin \phi \cdot r \cdot \sin \theta_s \cdot \sin \phi + r \cdot \cos \theta_t \cdot r \cdot \cos \theta_s}{r \cdot r} \\ &= \sin \theta_t \cdot \cos \phi \cdot \sin \theta_s \cdot \cos \phi + \sin \theta_t \cdot \sin \phi \cdot \sin \theta_s \cdot \sin \phi + \cos \theta_t \cdot \cos \theta_s \\ &= \sin \theta_t \cdot \sin \theta_s (\cos^2 \phi + \sin^2 \phi) + \cos \theta_t \cdot \cos \theta_s \\ &= \cos(\theta_t - \theta_s) \\ &= \cos(\Delta\theta) \end{aligned}$$

The cosine similarity between $\nu^{(t)}$ and $\nu^{(s)}$ is, in fact, given by $\cos(\Delta\theta)$, where $\Delta\theta$ represents the angular difference between the two vectors. By adjusting $\Delta\theta$ to be uniformly distributed between -1 and 1, we can effectively control the quality of the source data, ranging from extremely poor to extremely good (i.e., having the same distribution as the target data).

For dimensions $d \geq 3$, we can employ a similar method to extend the concept to higher-dimensional spaces.

We define a coordinate system in an n -dimensional Euclidean space that generalizes the spherical coordinate system used in three-dimensional Euclidean space. In this system, the coordinates are composed of a radial coordinate r and $n - 1$ angular coordinates $\varphi_1, \varphi_2, \dots, \varphi_{n-1}$. If x_i are the Cartesian coordinates, i.e. $\nu^{(t)} = (x_1^{(t)}, \dots, x_n^{(t)})$, then we can compute $r, \varphi_1^{(t)}, \varphi_2, \dots, \varphi_{n-1}$ using the following transformations:

$$\begin{aligned} r &= \sqrt{(x_1^{(t)})^2 + (x_2^{(t)})^2 + \dots + (x_{n-1}^{(t)})^2 + (x_n^{(t)})^2}, \\ \varphi_1^{(t)} &= \arccos\left(\frac{x_1^{(t)}}{r}\right), \\ \varphi_2 &= \arccos\left(\frac{x_2^{(t)}}{r \sin(\varphi_1)}\right), \\ &\vdots \\ \varphi_{n-2} &= \arccos\left(\frac{x_{n-2}^{(t)}}{r \sin(\varphi_1) \cdots \sin(\varphi_{n-3})}\right), \\ \varphi_{n-1} &= \arccos\left(\frac{x_{n-1}^{(t)}}{r \sin(\varphi_1) \cdots \sin(\varphi_{n-2})}\right). \end{aligned}$$

Following the same procedure as outlined above, we modify the angle φ_1 to $\varphi_1^{(s)}$ by applying an angular shift $\Delta\varphi_1$, such that:

$$\varphi_1^{(s)} = \varphi_1 - \Delta\varphi_1.$$

and we keep the $r, \varphi_2, \dots, \varphi_{n-1}$ unchanged.

The Cartesian coordinates can then be reconstructed using the modified angle $\varphi_1^{(s)}$ for the source data:

$$\begin{aligned} x_1^{(s)} &= r \cos(\varphi_1^{(s)}), \\ x_2^{(s)} &= r \sin(\varphi_1^{(s)}) \cos(\varphi_2), \\ x_3^{(s)} &= r \sin(\varphi_1^{(s)}) \sin(\varphi_2) \cos(\varphi_3), \\ &\vdots \\ x_{n-1}^{(s)} &= r \sin(\varphi_1^{(s)}) \cdots \sin(\varphi_{n-2}) \cos(\varphi_{n-1}), \\ x_n^{(s)} &= r \sin(\varphi_1^{(s)}) \cdots \sin(\varphi_{n-2}) \sin(\varphi_{n-1}). \end{aligned}$$

and

$$\nu^{(s)} = (x_1^{(s)}, x_2^{(s)}, \dots, x_{n-1}^{(s)}, x_n^{(s)})$$

Consequently, we arrive at a similar conclusion, where the cosine similarity is given by $S_C(\nu^{(t)}, \nu^{(s)}) = \cos(\Delta\varphi_1)$.

B.2 Synthetic Data Generation for Binary Classification

In the binary classification experiments, we consider five generative settings: (i) logistic regression; (ii) probit model regression; (iii) LDA; (iv) QDA; (v) mixture Gaussian model.

For CLS estimation, we consider four models for binary classification: logistic regression, linear SVM, radial SVM, XGBoost.

B.2.1 Logistic Regression Setting

We consider a commonly utilized linear classifier-logistic regression. Each sample $\mathbf{x}_i^{(t)}$ and $\mathbf{x}_i^{(s)}$ is independently drawn from $\mathcal{N}_p(0, \Sigma)$, where $i = 1, \dots, n_t$ for the target data and $i = 1, \dots, n_s$ for the source data. The covariance matrix Σ has an auto-regression correlation structure, specifically $\Sigma = (0.5^{|r-c|})_{p \times p}$ for feature indices $r, c = 1, \dots, p$ and feature dimension $p = 10$. For the target data, each binary outcome is generated according to a Bernoulli distribution, where the probability is given by:

$$P(y_i = 1) = \frac{1}{1 + \exp(-\pi_i)},$$

where $\pi_i = \beta^{(t)\top} \mathbf{x}_i$, and coefficient vector $\beta^{(t)}$ is drawn from $\mathcal{N}_p(\frac{1}{4}\mathbf{1}, \frac{1}{16}\mathbf{I}_p)$, where $\mathbf{1}$ denotes a p -dimensional vector of ones, and \mathbf{I}_p denotes the $p \times p$ identity matrix. The binary responses in the source datasets are generated similarly, but with varying coefficients: we generate $\beta^{(s)}$ using the method described in Section B.1 in order to control the cosine similarity between $\beta^{(t)}$ and $\beta^{(s)}$.

The Oracle CLS is calculated using $\beta^{(t)}, \beta^{(s)}$ based on the above data generation mechanism.

All results for this setting are presented in Figure 8, Table 4, Table 5, and Figure 9.

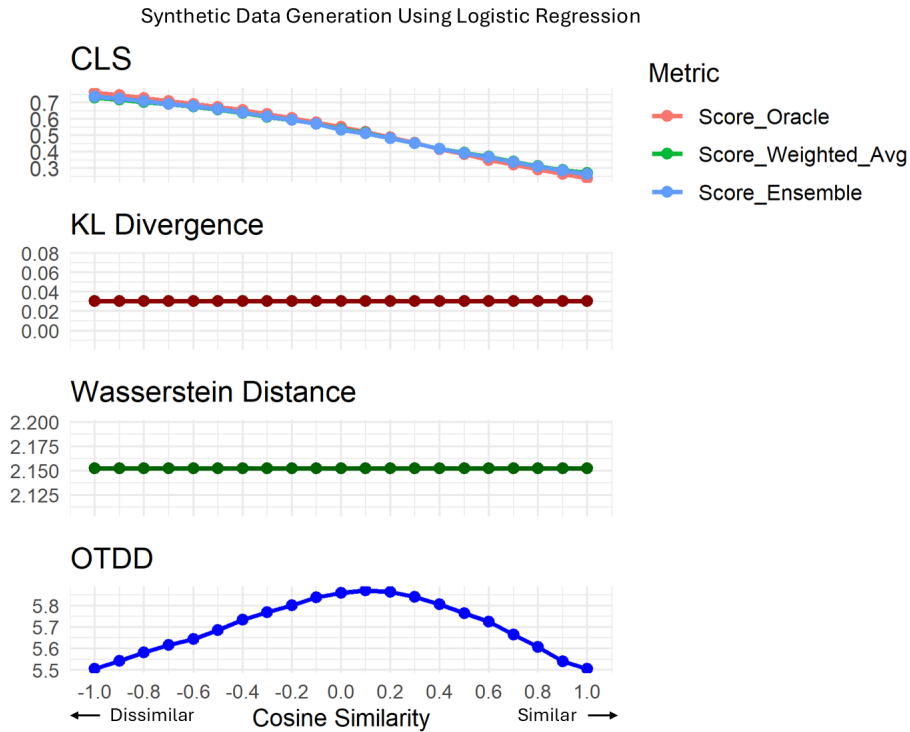


Figure 8: Comparison of CLS vs other similarity metrics under the Logistic Regression Setting

B.2.2 Probit Model Setting

Consider a binary classification problem where the features $\mathbf{x}_i \in \mathbb{R}^p$ (for sample index $i = 1, \dots, n_t$ for the target dataset and $i = 1, \dots, n_s$ for the source dataset) are independently and identically distributed (i.i.d.) as $\mathbf{x}_i \sim \mathcal{N}_p(0, \mathbf{I}_p)$, and the relationship between features and labels follows a linear model

$$y_i = \mathbb{I}[(\beta^\top \mathbf{x}_i + \xi_i) \geq 0],$$

where $\beta \in \mathbb{R}^p$ is the parameter vector, $\xi_i \sim \mathcal{N}(0, 1)$ is a random noise term, and $\mathbb{I}[\cdot]$ denotes the indicator function. This formulation corresponds to the Probit model.

We consider two datasets: the target dataset, characterized by the parameter vector $\beta^{(t)}$, and the source dataset, characterized by the parameter vector $\beta^{(s)}$. We replace β in the above linear Probit model with $\beta^{(t)}$ and $\beta^{(s)}$ to generate

Cosine Sim.	Score Oracle	Score Unw. Avg	Score Wtd. Avg	Score Ens.	KL Div.	Wass. Dist.	OTDD
-1.0	0.7629	0.7288	0.7311	0.7370	0.0304	2.1526	5.5051
-0.9	0.7469	0.7179	0.7199	0.7245	0.0304	2.1526	5.5423
-0.8	0.7285	0.7030	0.7050	0.7094	0.0304	2.1526	5.5806
-0.7	0.7087	0.6890	0.6905	0.6926	0.0304	2.1526	5.6159
-0.6	0.6911	0.6755	0.6771	0.6785	0.0304	2.1526	5.6432
-0.5	0.6743	0.6576	0.6592	0.6620	0.0304	2.1526	5.6856
-0.4	0.6560	0.6356	0.6371	0.6399	0.0304	2.1526	5.7333
-0.3	0.6306	0.6123	0.6130	0.6150	0.0304	2.1526	5.7699
-0.2	0.6067	0.5922	0.5933	0.5943	0.0304	2.1526	5.8024
-0.1	0.5787	0.5688	0.5697	0.5692	0.0304	2.1526	5.8380
0.0	0.5521	0.5370	0.5373	0.5350	0.0304	2.1526	5.8587
0.1	0.5212	0.5153	0.5155	0.5140	0.0304	2.1526	5.8705
0.2	0.4872	0.4840	0.4834	0.4837	0.0304	2.1526	5.8646
0.3	0.4535	0.4523	0.4517	0.4527	0.0304	2.1526	5.8415
0.4	0.4150	0.4204	0.4196	0.4185	0.0304	2.1526	5.8066
0.5	0.3846	0.3956	0.3942	0.3922	0.0304	2.1526	5.7643
0.6	0.3501	0.3711	0.3698	0.3670	0.0304	2.1526	5.7260
0.7	0.3220	0.3403	0.3384	0.3362	0.0304	2.1526	5.6658
0.8	0.2909	0.3160	0.3130	0.3098	0.0304	2.1526	5.6076
0.9	0.2623	0.2920	0.2895	0.2840	0.0304	2.1526	5.5399
1.0	0.2371	0.2712	0.2689	0.2630	0.0304	2.1526	5.5051
$ \rho_p $	0.9937	0.9945	0.9945	0.9948	0.0000	0.0000	0.1351
$ \rho_s $	1.0000	1.0000	1.0000	1.0000	0.0000	0.0000	0.1143

Table 4: Comparison of similarity metrics across varying cosine similarity values under the Logistic Regression setting

Cosine Similar.	Logistic Regr.	SVM Linear	SVM Radial	Xgb Tree	Score Unw. Avg	Score Wtd. Avg	Score Ens.	Score Oracle
-1.0	0.7392	0.7362	0.7347	0.7050	0.7288	0.7311	0.7370	0.7629
-0.9	0.7268	0.7242	0.7233	0.6972	0.7179	0.7199	0.7245	0.7469
-0.8	0.7124	0.7094	0.7086	0.6814	0.7030	0.7050	0.7094	0.7285
-0.7	0.6956	0.6941	0.6944	0.6719	0.6890	0.6905	0.6926	0.7087
-0.6	0.6812	0.6808	0.6810	0.6588	0.6755	0.6771	0.6785	0.6911
-0.5	0.6629	0.6632	0.6610	0.6432	0.6576	0.6592	0.6620	0.6743
-0.4	0.6399	0.6397	0.6394	0.6236	0.6356	0.6371	0.6399	0.6560
-0.3	0.6142	0.6140	0.6177	0.6032	0.6123	0.6130	0.6150	0.6306
-0.2	0.5956	0.5940	0.5980	0.5811	0.5922	0.5933	0.5943	0.6067
-0.1	0.5710	0.5710	0.5741	0.5588	0.5688	0.5697	0.5692	0.5787
0.0	0.5384	0.5356	0.5410	0.5329	0.5370	0.5373	0.5350	0.5521
0.1	0.5152	0.5134	0.5150	0.5174	0.5153	0.5155	0.5140	0.5212
0.2	0.4832	0.4823	0.4808	0.4897	0.4840	0.4834	0.4837	0.4872
0.3	0.4500	0.4519	0.4475	0.4600	0.4523	0.4517	0.4527	0.4535
0.4	0.4196	0.4178	0.4132	0.4310	0.4204	0.4196	0.4185	0.4150
0.5	0.3918	0.3920	0.3883	0.4105	0.3956	0.3942	0.3922	0.3846
0.6	0.3660	0.3676	0.3622	0.3888	0.3711	0.3698	0.3670	0.3501
0.7	0.3342	0.3335	0.3325	0.3611	0.3403	0.3384	0.3362	0.3220
0.8	0.3064	0.3082	0.3098	0.3396	0.3160	0.3130	0.3098	0.2909
0.9	0.2818	0.2840	0.2844	0.3180	0.2920	0.2895	0.2840	0.2623
1.0	0.2608	0.2638	0.2653	0.2950	0.2712	0.2689	0.2630	0.2371
Diff.	0.0129	0.0140	0.0133	0.0321	0.0178	0.0165	0.0142	-

Table 5: Diff between \widehat{CLS} and oracle CLS under the Logistic Regression setting

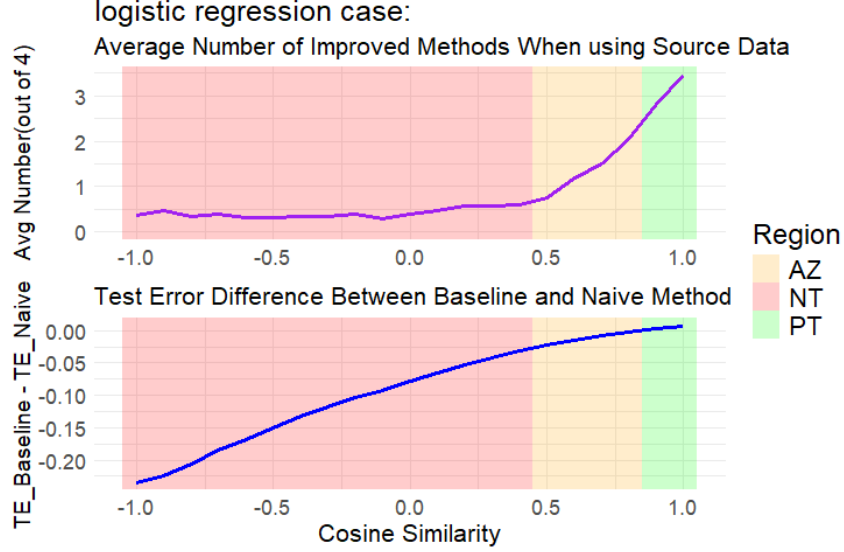


Figure 9: Transferability zones (positive, ambiguous, and negative) identified under the logistic regression model

the target and source datasets, respectively. The coefficient vector $\beta^{(t)}$ for the target data is drawn from $\mathcal{N}_p(\frac{1}{4}\mathbf{1}, \frac{1}{16}\mathbf{I}_p)$, where $\mathbf{1}$ denotes a p -dimensional vector of ones and \mathbf{I}_p denotes the $p \times p$ identity matrix. The vector $\beta^{(s)}$ is generated using the method described in Section B.1 to control the cosine similarity between $\beta^{(t)}$ and $\beta^{(s)}$. We set the feature dimension $p = 10$.

The Oracle CLS is computed using the formula derived in the proof of Theorem 1.

All results for this setting are presented in Figure 10, Table 6, Table 7, and Figure 11.

Cosine Sim.	Score Oracle	Score Unw. Avg	Score Wtd. Avg	Score Ens.	KL Div.	Wass. Dist.	OTDD
-1.0	0.7705	0.7357	0.7439	0.7506	0.0304	2.3909	6.6073
-0.9	0.7363	0.7073	0.7128	0.7200	0.0304	2.3909	6.6403
-0.8	0.7052	0.6837	0.6884	0.6938	0.0304	2.3909	6.6685
-0.7	0.6762	0.6597	0.6637	0.6697	0.0304	2.3909	6.6962
-0.6	0.6488	0.6337	0.6376	0.6423	0.0304	2.3909	6.7245
-0.5	0.6226	0.6093	0.6132	0.6159	0.0304	2.3909	6.7477
-0.4	0.5971	0.5857	0.5886	0.5906	0.0304	2.3909	6.7674
-0.3	0.5723	0.5649	0.5675	0.5674	0.0304	2.3909	6.7811
-0.2	0.5480	0.5420	0.5441	0.5420	0.0304	2.3909	6.7931
-0.1	0.5239	0.5178	0.5194	0.5186	0.0304	2.3909	6.8007
0.0	0.5000	0.4949	0.4958	0.4938	0.0304	2.3909	6.8049
0.1	0.4761	0.4727	0.4733	0.4722	0.0304	2.3909	6.8040
0.2	0.4520	0.4550	0.4551	0.4538	0.0304	2.3909	6.8005
0.3	0.4277	0.4347	0.4342	0.4328	0.0304	2.3909	6.7912
0.4	0.4029	0.4126	0.4115	0.4083	0.0304	2.3909	6.7764
0.5	0.3774	0.3900	0.3885	0.3884	0.0304	2.3909	6.7607
0.6	0.3512	0.3674	0.3655	0.3647	0.0304	2.3909	6.7390
0.7	0.3238	0.3437	0.3412	0.3398	0.0304	2.3909	6.7137
0.8	0.2948	0.3184	0.3148	0.3108	0.0304	2.3909	6.6821
0.9	0.2637	0.2954	0.2905	0.2846	0.0304	2.3909	6.6513
1.0	0.2295	0.2652	0.2587	0.2516	0.0304	2.3909	6.6080
$ \rho_p $	0.9993	0.9996	0.9995	0.9993	0.0000	0.0000	0.0697
$ \rho_s $	1.0000	1.0000	1.0000	1.0000	0.0000	0.0000	0.0714

Table 6: Comparison of similarity metrics across varying cosine similarity values under the Probit Model setting

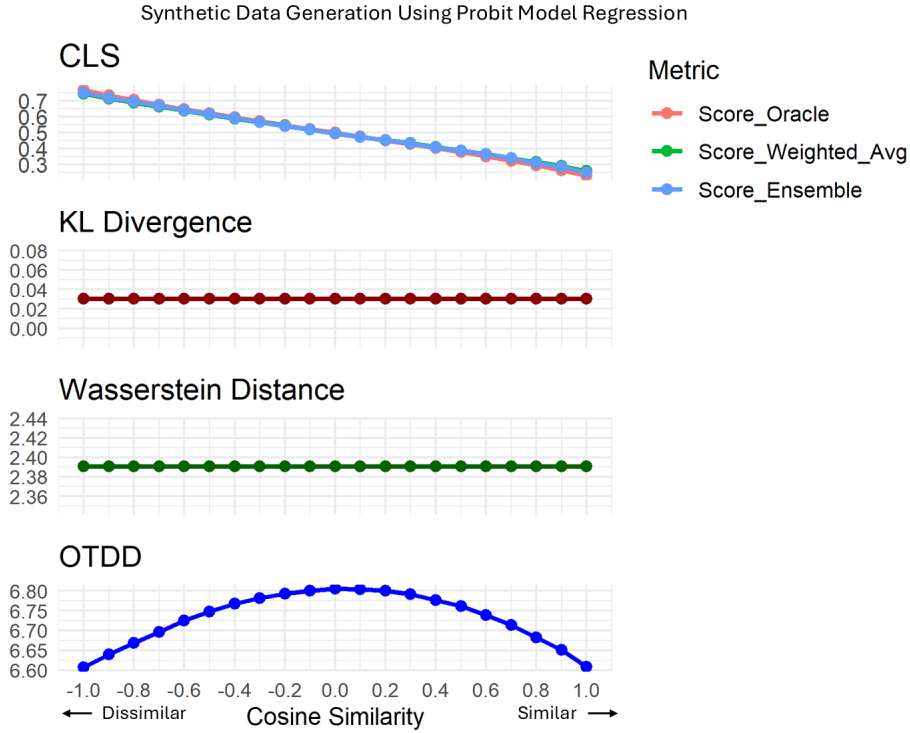


Figure 10: Comparison of CLS vs other similarity metrics under the Probit Model

Cos. Sim.	Probit	Log. Regr.	SVM Linear	SVM Radial	Xgb Tree	Score Unw. Avg	Score Wtd. Avg	Score Ens.	Score Oracle
-1.0	0.7566	0.7568	0.7552	0.7314	0.6994	0.7357	0.7439	0.7506	0.7705
-0.9	0.7234	0.7242	0.7226	0.7056	0.6768	0.7073	0.7128	0.7200	0.7363
-0.8	0.6978	0.6978	0.6976	0.6819	0.6572	0.6837	0.6884	0.6938	0.7052
-0.7	0.6732	0.6736	0.6712	0.6572	0.6367	0.6597	0.6637	0.6697	0.6762
-0.6	0.6472	0.6476	0.6445	0.6320	0.6108	0.6337	0.6376	0.6423	0.6488
-0.5	0.6197	0.6208	0.6200	0.6102	0.5862	0.6093	0.6132	0.6159	0.6226
-0.4	0.5956	0.5961	0.5957	0.5868	0.5641	0.5857	0.5886	0.5906	0.5971
-0.3	0.5728	0.5734	0.5728	0.5673	0.5459	0.5649	0.5675	0.5674	0.5723
-0.2	0.5498	0.5494	0.5480	0.5446	0.5259	0.5420	0.5441	0.5420	0.5480
-0.1	0.5247	0.5248	0.5222	0.5187	0.5054	0.5178	0.5194	0.5186	0.5239
0.0	0.4986	0.4998	0.4992	0.4960	0.4848	0.4949	0.4958	0.4938	0.5000
0.1	0.4757	0.4758	0.4744	0.4744	0.4662	0.4727	0.4733	0.4722	0.4761
0.2	0.4562	0.4566	0.4566	0.4566	0.4504	0.4550	0.4551	0.4538	0.4520
0.3	0.4338	0.4343	0.4339	0.4352	0.4355	0.4347	0.4342	0.4328	0.4277
0.4	0.4092	0.4095	0.4110	0.4128	0.4170	0.4126	0.4115	0.4083	0.4029
0.5	0.3850	0.3857	0.3850	0.3900	0.3995	0.3900	0.3885	0.3884	0.3774
0.6	0.3598	0.3607	0.3608	0.3672	0.3808	0.3674	0.3655	0.3647	0.3512
0.7	0.3348	0.3353	0.3350	0.3441	0.3605	0.3437	0.3412	0.3398	0.3238
0.8	0.3054	0.3063	0.3082	0.3193	0.3400	0.3184	0.3148	0.3108	0.2948
0.9	0.2788	0.2790	0.2818	0.2980	0.3230	0.2954	0.2905	0.2846	0.2637
1.0	0.2448	0.2450	0.2490	0.2636	0.3033	0.2652	0.2587	0.2516	0.2295
Diff.	0.0063	0.0063	0.0073	0.0159	0.0337	0.0157	0.0127	0.0101	-

Table 7: Diff between \widehat{CLS} and oracle CLS under the Probit Model setting

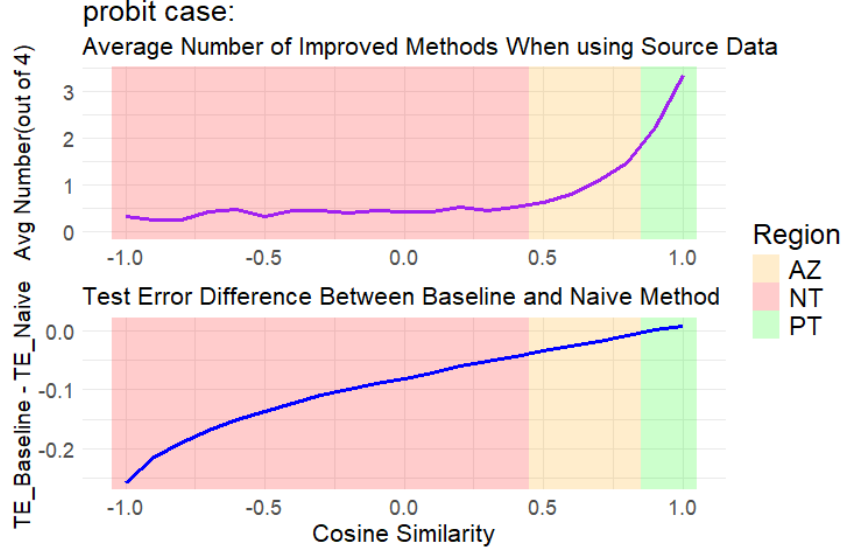


Figure 11: Transferability zones (positive, ambiguous, and negative) identified under the probit model

B.2.3 Linear Discriminant Analysis(LDA) Setting

We consider a simple Linear Discriminant Analysis (LDA) setting. We generate the target dataset with n_t i.i.d. samples $\{(\mathbf{x}_i^{(t)}, y_i^{(t)})\}_{i=1}^{n_t}$, and the source dataset with n_s i.i.d. samples $\{(\mathbf{x}_i^{(s)}, y_i^{(s)})\}_{i=1}^{n_s}$, and we set the feature dimension $p = 10$. The class labels take values in $\{0, 1\}$, and for both datasets, we assign exactly half of the samples to each class in order to ensure perfect class balance and reduce label variance during evaluation.

Conditional on the class label $l \in \{0, 1\}$, the features follow Gaussian distributions:

$$\mathbf{X}_i^{(t)} | Y_i^{(t)} = l \sim \mathcal{N}_p \left((-1)^{1-l} \mu^{(t)}, I_p \right), \quad \mathbf{X}_i^{(s)} | Y_i^{(s)} = l \sim \mathcal{N}_p \left((-1)^{1-l} \mu^{(s)}, I_p \right),$$

where $\mu^{(t)}, \mu^{(s)} \in \mathbb{R}^p$ are the class means for the target and source data, respectively, and I_p is the $p \times p$ identity matrix.

The coefficient vector $\mu^{(t)}$ for target data is set to $\mu^{(t)} = (0.3, 0.3, \dots, 0.3) \in \mathbb{R}^p$. The vector $\mu^{(s)}$ is generated using the method described in Section B.1 to control the cosine similarity between $\mu^{(t)}$ and $\mu^{(s)}$.

The Oracle CLS is derived in Theorem 2.

All results for this setting are presented in Table 8, Table 9, Figure 12, and Figure 13.

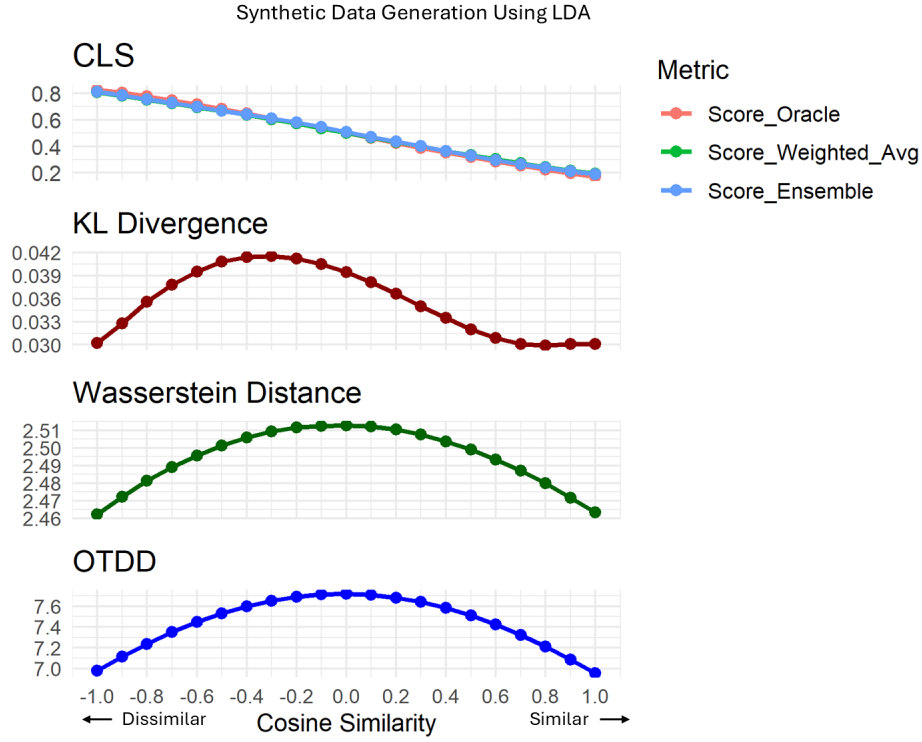


Figure 12: Comparison of CLS vs other similarity metrics under the LDA setting

Cosine Sim.	Score Oracle	Score Unw. Avg	Score Wtd. Avg	Score Ens.	KL Div.	Wass. Dist.	OTDD
-1.0	0.8286	0.7997	0.8074	0.8131	0.0302	2.4621	6.9796
-0.9	0.8034	0.7744	0.7801	0.7864	0.0328	2.4722	7.1154
-0.8	0.7761	0.7474	0.7519	0.7562	0.0356	2.4814	7.2374
-0.7	0.7467	0.7202	0.7241	0.7269	0.0378	2.4891	7.3492
-0.6	0.7154	0.6929	0.6954	0.6986	0.0395	2.4958	7.4472
-0.5	0.6824	0.6649	0.6672	0.6684	0.0408	2.5015	7.5305
-0.4	0.6478	0.6349	0.6363	0.6410	0.0414	2.5060	7.5992
-0.3	0.6120	0.6036	0.6044	0.6101	0.0415	2.5094	7.6521
-0.2	0.5752	0.5713	0.5723	0.5786	0.0412	2.5116	7.6894
-0.1	0.5378	0.5365	0.5366	0.5451	0.0405	2.5126	7.7122
0.0	0.5000	0.5025	0.5024	0.5098	0.0394	2.5129	7.7179
0.1	0.4622	0.4688	0.4680	0.4716	0.0381	2.5123	7.7082
0.2	0.4248	0.4356	0.4339	0.4376	0.0366	2.5105	7.6812
0.3	0.3880	0.4031	0.4001	0.4009	0.0350	2.5077	7.6396
0.4	0.3522	0.3702	0.3658	0.3658	0.0335	2.5038	7.5833
0.5	0.3176	0.3379	0.3326	0.3282	0.0320	2.4991	7.5105
0.6	0.2846	0.3089	0.3032	0.2961	0.0309	2.4934	7.4232
0.7	0.2533	0.2784	0.2723	0.2646	0.0301	2.4872	7.3223
0.8	0.2239	0.2490	0.2426	0.2378	0.0299	2.4800	7.2098
0.9	0.1966	0.2239	0.2175	0.2122	0.0301	2.4717	7.0863
1.0	0.1714	0.2012	0.1950	0.1884	0.0301	2.4635	6.9550
$ \rho_p $	0.9992	0.9994	0.9994	0.9992	0.5155	0.0274	0.0408
$ \rho_s $	1.0000	1.0000	1.0000	1.0000	0.5545	0.0455	0.0714

Table 8: Comparison of similarity metrics across varying cosine similarity values under the LDA setting

Cos. Sim.	LDA	Log. Repr.	SVM Linear	SVM Radial	Xgb Tree	Score Unw. Avg	Score Wtd. Avg	Score Ens.	Score Oracle
-1.0	0.8154	0.8159	0.8158	0.8049	0.7621	0.7997	0.8074	0.8131	0.8286
-0.9	0.7901	0.7884	0.7900	0.7806	0.7384	0.7744	0.7801	0.7864	0.8034
-0.8	0.7621	0.7606	0.7612	0.7541	0.7136	0.7474	0.7519	0.7562	0.7761
-0.7	0.7350	0.7336	0.7321	0.7270	0.6880	0.7202	0.7241	0.7269	0.7467
-0.6	0.7064	0.7034	0.7027	0.6984	0.6668	0.6929	0.6954	0.6986	0.7154
-0.5	0.6738	0.6739	0.6753	0.6682	0.6424	0.6649	0.6672	0.6684	0.6824
-0.4	0.6429	0.6420	0.6407	0.6358	0.6210	0.6349	0.6363	0.6410	0.6478
-0.3	0.6099	0.6064	0.6102	0.6020	0.5958	0.6036	0.6044	0.6101	0.6120
-0.2	0.5730	0.5741	0.5741	0.5656	0.5714	0.5713	0.5723	0.5786	0.5752
-0.1	0.5376	0.5366	0.5354	0.5284	0.5456	0.5365	0.5366	0.5451	0.5378
0.0	0.4986	0.4997	0.4992	0.4929	0.5184	0.5025	0.5024	0.5098	0.5000
0.1	0.4625	0.4624	0.4642	0.4578	0.4908	0.4688	0.4680	0.4716	0.4622
0.2	0.4258	0.4254	0.4278	0.4261	0.4630	0.4356	0.4339	0.4376	0.4248
0.3	0.3919	0.3922	0.3926	0.3922	0.4353	0.4031	0.4001	0.4009	0.3880
0.4	0.3586	0.3580	0.3596	0.3606	0.4026	0.3702	0.3658	0.3658	0.3522
0.5	0.3253	0.3248	0.3256	0.3298	0.3715	0.3379	0.3326	0.3282	0.3176
0.6	0.2928	0.2939	0.2961	0.3035	0.3422	0.3089	0.3032	0.2961	0.2846
0.7	0.2632	0.2644	0.2653	0.2734	0.3105	0.2784	0.2723	0.2646	0.2533
0.8	0.2354	0.2357	0.2342	0.2456	0.2806	0.2490	0.2426	0.2378	0.2239
0.9	0.2103	0.2102	0.2104	0.2211	0.2542	0.2239	0.2175	0.2122	0.1966
1.0	0.1864	0.1878	0.1875	0.1968	0.2329	0.2012	0.1950	0.1884	0.1714
Diff.	0.0075	0.0081	0.0084	0.0147	0.0439	0.0183	0.0147	0.0124	-

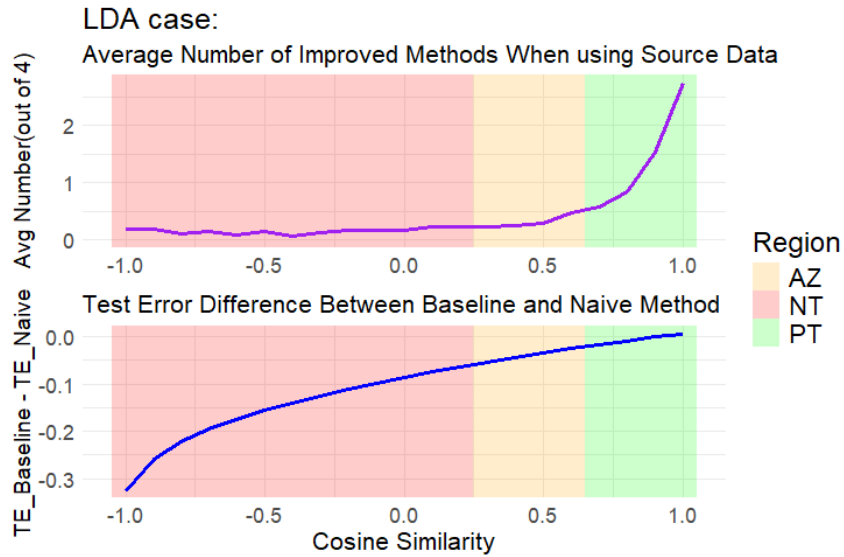
Table 9: Diff between \widehat{CLS} and oracle CLS under the LDA setting

Figure 13: Transferability zones (positive, ambiguous, and negative) identified under the LDA model

B.2.4 Mixture Gaussian Setting

We consider a binary classification setting under a mixture gaussian model with feature dimension $p = 10$. The label space is $\{0, 1\}$, and we generate both target and source datasets.

For the target dataset, we generate n_t i.i.d. samples $\{(\mathbf{X}_i^{(t)}, Y_i^{(t)})\}_{i=1}^{n_t}$, where the class-conditional distributions are:

$$\mathbf{X}_i^{(t)} | Y_i^{(t)} = 1 \sim \mathcal{N}_p(\mu^{(t)}, I_p), \quad \mathbf{X}_i^{(t)} | Y_i^{(t)} = 0 \sim \mathcal{N}_p(-\mu^{(t)}, I_p),$$

with the class mean defined as $\mu^{(t)} = (0.3, 0.3, \dots, 0.3) \in \mathbb{R}^p$, and I_p being the 10×10 identity matrix.

For the source dataset, we generate n_s i.i.d. samples $\{(\mathbf{X}_i^{(s)}, Y_i^{(s)})\}_{i=1}^{n_s}$, where the class-conditional distribution is modeled as a probabilistic mixture of the target and source Gaussian components, controlled by a shift parameter $\alpha \in [0, 1]$:

$$\begin{aligned} \mathbf{X}_i^{(s)} | Y_i^{(s)} = 1 &\sim (1 - \alpha) \mathcal{N}_p(\mu^{(t)}, I_p) + \alpha \mathcal{N}_p(\mu^{(s)}, I_p), \\ \mathbf{X}_i^{(s)} | Y_i^{(s)} = 0 &\sim (1 - \alpha) \mathcal{N}_p(-\mu^{(t)}, I_p) + \alpha \mathcal{N}_p(-\mu^{(s)}, I_p), \end{aligned}$$

where $\mu^{(s)} \in \mathbb{R}^p$ is the source class-1 mean, each coordinate of $\mu^{(s)}$ is sampled independently from $\mathcal{N}(-0.3, 0.5^2)$.

This construction introduces a controllable distribution shift parameter α between the target and source datasets. Here, the shift parameter α serves as a controllable factor determining the degree of domain divergence. When $\alpha = 0$, the source distribution matches the target exactly; as α increases, the source data diverge due to increasing influence from the shifted Gaussian components.

The Oracle CLS is calculated using $\mu^{(t)}, \mu^{(s)}, \alpha$ based on the above data generation mechanism.

All results for this setting are presented in Table 10, Table 11, Figure 14, and Figure 15.

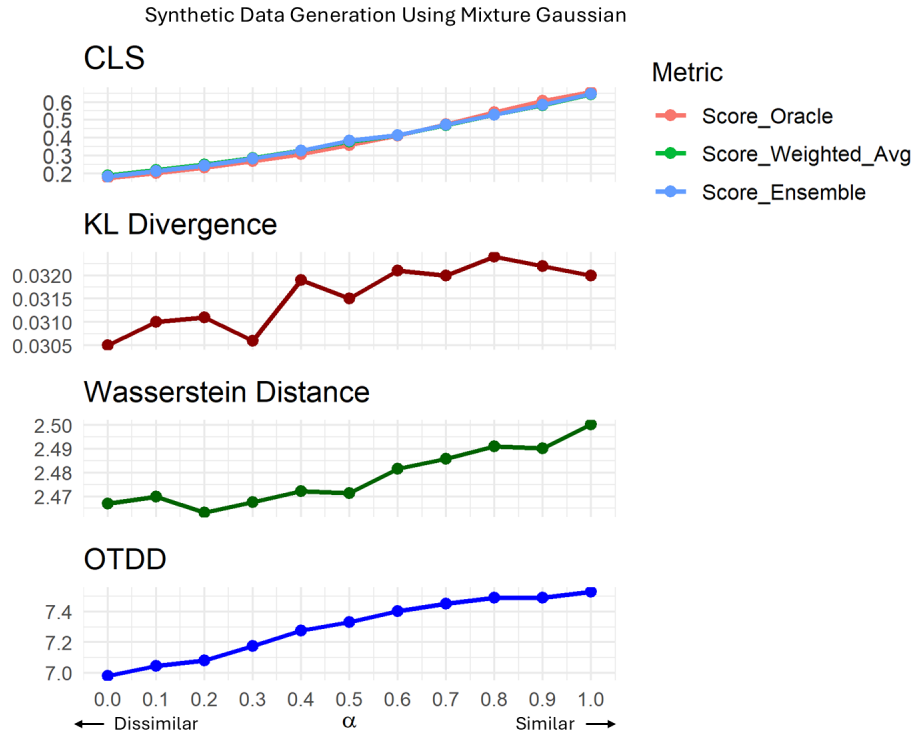


Figure 14: Comparison of CLS vs other similarity metrics under the Mixture Gaussian Model

B.2.5 Quadratic Discriminant Analysis (QDA) Setting

We consider a Quadratic Discriminant Analysis (QDA) setting for synthetic data generation. We generate the target dataset with n_t i.i.d. samples $\{(\mathbf{x}_i^{(t)}, y_i^{(t)})\}_{i=1}^{n_t}$, and the source dataset with n_s i.i.d. samples $\{(\mathbf{x}_i^{(s)}, y_i^{(s)})\}_{i=1}^{n_s}$, and we

Alpha	Score Oracle	Score Unw. Avg	Score Wtd. Avg	Score Ens.	KL Div.	Wass. Dist.	OTDD
0.0	0.1745	0.1958	0.1889	0.1829	0.0305	2.4670	6.9780
0.1	0.2023	0.2231	0.2179	0.2133	0.0310	2.4698	7.0457
0.2	0.2317	0.2549	0.2499	0.2446	0.0311	2.4631	7.0804
0.3	0.2685	0.2892	0.2866	0.2837	0.0306	2.4675	7.1756
0.4	0.3082	0.3304	0.3273	0.3266	0.0319	2.4722	7.2742
0.5	0.3586	0.3782	0.3785	0.3823	0.0315	2.4714	7.3297
0.6	0.4126	0.4162	0.4142	0.4132	0.0321	2.4816	7.4034
0.7	0.4766	0.4740	0.4715	0.4718	0.0320	2.4858	7.4521
0.8	0.5438	0.5277	0.5280	0.5304	0.0324	2.4911	7.4903
0.9	0.6067	0.5816	0.5821	0.5849	0.0322	2.4903	7.4896
1.0	0.6589	0.6417	0.6441	0.6474	0.0320	2.5003	7.5307
$ \rho_p $	0.9906	0.9938	0.9941	0.9945	0.8639	0.9345	0.9817
$ \rho_s $	1.0000	1.0000	1.0000	1.0000	0.8545	0.9364	0.9909

Table 10: Comparison of similarity metrics across varying α values under the Mixture Gaussian setting

Alpha	LDA	Log. Regr.	SVM Linear	SVM Radial	Xgb Tree	Score Unw. Avg	Score Wtd. Avg	Score Ens.	Score Oracle
0.0	0.1803	0.1814	0.1826	0.1910	0.2282	0.1958	0.1889	0.1829	0.1745
0.1	0.2089	0.2112	0.2110	0.2175	0.2526	0.2231	0.2179	0.2133	0.2023
0.2	0.2392	0.2412	0.2414	0.2497	0.2874	0.2549	0.2499	0.2446	0.2317
0.3	0.2784	0.2796	0.2782	0.2822	0.3166	0.2892	0.2866	0.2837	0.2685
0.4	0.3164	0.3166	0.3204	0.3286	0.3560	0.3304	0.3273	0.3266	0.3082
0.5	0.3662	0.3674	0.3660	0.3820	0.3975	0.3782	0.3785	0.3823	0.3586
0.6	0.4082	0.4071	0.4060	0.4207	0.4311	0.4162	0.4142	0.4132	0.4126
0.7	0.4672	0.4669	0.4699	0.4804	0.4788	0.4740	0.4715	0.4718	0.4766
0.8	0.5282	0.5260	0.5274	0.5338	0.5237	0.5277	0.5280	0.5304	0.5438
0.9	0.5868	0.5843	0.5819	0.5886	0.5718	0.5816	0.5821	0.5849	0.6067
1.0	0.6480	0.6480	0.6471	0.6460	0.6254	0.6417	0.6441	0.6474	0.6589
Diff.	0.0096	0.0109	0.0111	0.0146	0.0367	0.0175	0.0152	0.0129	-

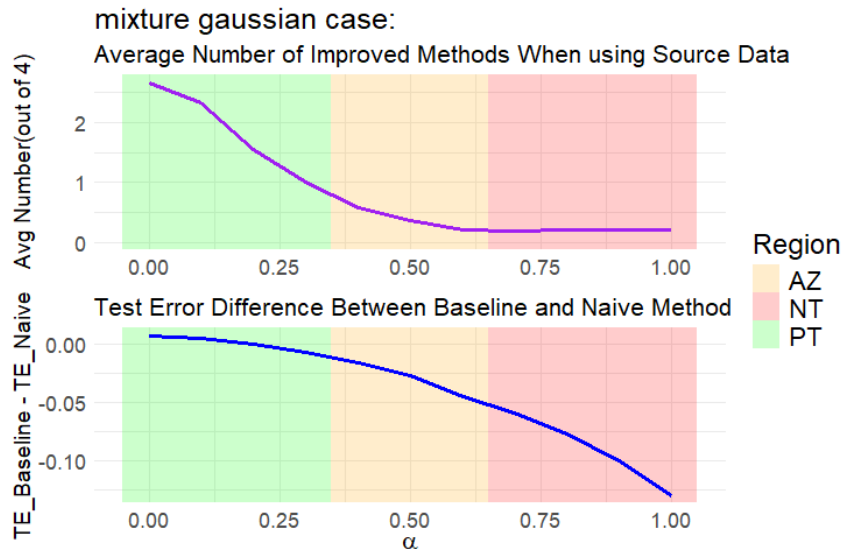
Table 11: Diff between \overline{CLS} and oracle CLS under the Mixture Gaussian setting

Figure 15: Transferability zones (positive, ambiguous, and negative) identified under the Mixture Gaussian model

set feature dimension $p = 10$. The class labels take values in $\{0, 1\}$, and for both datasets, we assign exactly half of the samples to each class to ensure perfect class balance during evaluation.

Conditional on the class label $l \in \{0, 1\}$, the features follow Gaussian distributions with class-specific covariance matrices:

$$\mathbf{X}_i^{(t)} | Y_i^{(t)} = l \sim \mathcal{N}_p \left((-1)^{1-l} \mu^{(t)}, \Sigma_l \right), \quad \mathbf{X}_i^{(s)} | Y_i^{(s)} = l \sim \mathcal{N}_p \left((-1)^{1-l} \mu^{(s)}, \Sigma_l \right),$$

where $\mu^{(t)}, \mu^{(s)} \in \mathbb{R}^p$ are the class means for the target and source data, respectively. The class-conditional covariance matrices are defined as:

$$\Sigma_0 = (0.7^{|r-c|})_{p \times p}, \quad \Sigma_1 = (0.3^{|r-c|})_{p \times p}.$$

where r and c index the feature dimensions, i.e., $r, c = 1, \dots, p$.

The coefficient vector $\mu^{(t)}$ for target data is set to $\mu^{(t)} = (0.4, 0.4, \dots, 0.4) \in \mathbb{R}^p$. The vector $\mu^{(s)}$ is generated using the method described in Section B.1 to control the cosine similarity between $\mu^{(t)}$ and $\mu^{(s)}$.

The Oracle CLS is calculated using $\mu^{(t)}, \mu^{(s)}, \Sigma_0, \Sigma_1$ based on the above data generation mechanism.

All results for this setting are presented in Table 12, Table 13, Figure 16, and Figure 17.

From Figure 16, we observe that the estimated CLS values (both the weighted-average and ensemble schemes) do not closely approximate the oracle. As shown in Table 13, the *Diff.* values of all four single models are relatively high compared with the optimal model (QDA), indicating that the selected models—logistic regression, linear SVM, radial SVM, and XGBoost—do not fit the data well. However, several patterns can still be identified: (1) for this nonlinear setting, nonlinear models (radial SVM and XGBoost) outperform linear ones; (2) the ensemble estimate (Ens.) achieves better performance than the weighted-average (Wtd. Avg.) and unweighted-average (Unw. Avg.) estimates; and (3) the estimated CLS values decrease monotonically as the cosine similarity increases.

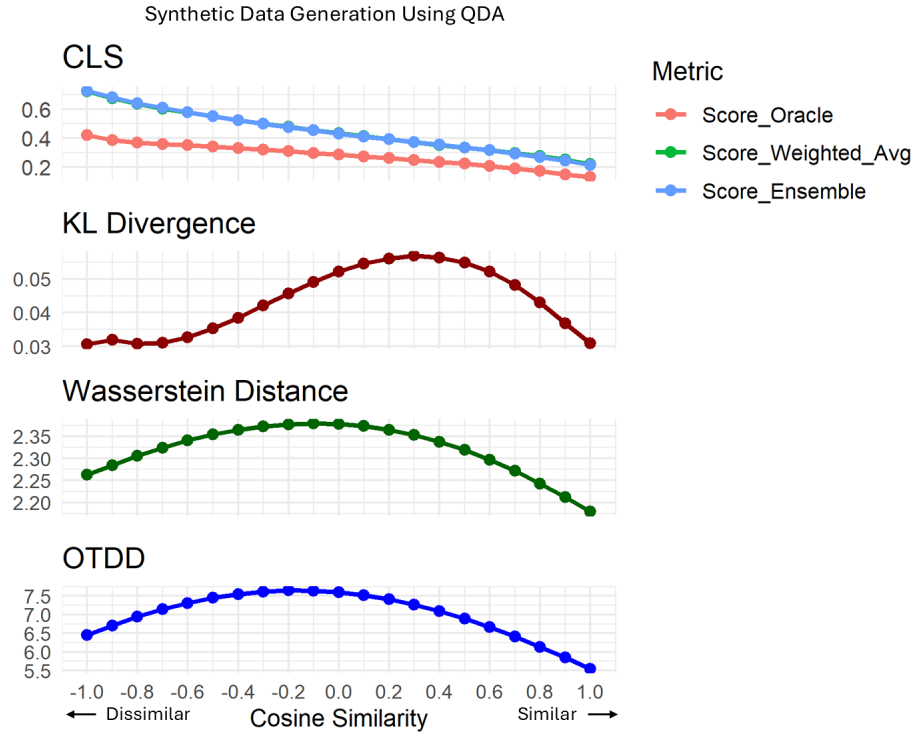


Figure 16: Comparison of CLS vs other similarity metrics under the QDA Setting

B.3 Synthetic Data Generation for Regression

For regression tasks, we consider two settings: (i) linear regression, and (ii) nonlinear regression, where features are generated using sinusoidal, polynomial, interaction, and exponential transformations with added Gaussian noise.

Cosine Sim.	Score Oracle	Score Unw. Avg	Score Wtd. Avg	Score Ens.	KL Div.	Wass. Dist.	OTDD
-1.0	0.4225	0.7332	0.7238	0.7302	0.0306	2.2624	6.4443
-0.9	0.3851	0.6834	0.6776	0.6844	0.0319	2.2849	6.7070
-0.8	0.3688	0.6422	0.6379	0.6436	0.0307	2.3057	6.9382
-0.7	0.3590	0.6091	0.6055	0.6102	0.0310	2.3244	7.1388
-0.6	0.3507	0.5822	0.5788	0.5794	0.0327	2.3405	7.3093
-0.5	0.3406	0.5551	0.5518	0.5518	0.0353	2.3541	7.4462
-0.4	0.3304	0.5302	0.5264	0.5251	0.0385	2.3649	7.5494
-0.3	0.3199	0.5065	0.5024	0.4998	0.0421	2.3727	7.6180
-0.2	0.3108	0.4835	0.4792	0.4772	0.0457	2.3776	7.6498
-0.1	0.2981	0.4621	0.4572	0.4556	0.0491	2.3796	7.6429
0.0	0.2865	0.4399	0.4349	0.4332	0.0522	2.3782	7.5992
0.1	0.2742	0.4190	0.4141	0.4126	0.0545	2.3735	7.5204
0.2	0.2626	0.3981	0.3930	0.3926	0.0561	2.3649	7.4086
0.3	0.2491	0.3786	0.3735	0.3736	0.0569	2.3528	7.2662
0.4	0.2353	0.3595	0.3539	0.3546	0.0564	2.3375	7.0915
0.5	0.2237	0.3416	0.3357	0.3344	0.0549	2.3190	6.8884
0.6	0.2089	0.3222	0.3162	0.3162	0.0522	2.2968	6.6610
0.7	0.1897	0.3030	0.2972	0.2948	0.0482	2.2715	6.4081
0.8	0.1718	0.2818	0.2756	0.2699	0.0431	2.2431	6.1340
0.9	0.1496	0.2567	0.2509	0.2452	0.0368	2.2119	5.8445
1.0	0.1320	0.2294	0.2217	0.2132	0.0309	2.1788	5.5427
$ \rho_p $	0.9934	0.9938	0.9947	0.9940	0.5027	-0.4149	-0.4970
$ \rho_s $	1.0000	1.0000	1.0000	1.0000	0.5078	-0.3026	-0.4234

Table 12: Comparison of similarity metrics across varying cosine similarity values under the QDA setting

Cos. Sim.	QDA	Log. Repr.	SVM Linear	SVM Radial	Xgb Tree	Score Unw. Avg	Score Wtd. Avg	Score Ens.	Score Oracle
-1.0	0.4606	0.7720	0.7682	0.7090	0.6838	0.7332	0.7238	0.7302	0.4225
-0.9	0.4308	0.7109	0.7130	0.6603	0.6492	0.6834	0.6776	0.6844	0.3851
-0.8	0.4152	0.6680	0.6695	0.6211	0.6102	0.6422	0.6379	0.6436	0.3688
-0.7	0.4007	0.6349	0.6350	0.5908	0.5758	0.6091	0.6055	0.6102	0.3590
-0.6	0.3878	0.6080	0.6088	0.5616	0.5504	0.5822	0.5788	0.5794	0.3507
-0.5	0.3765	0.5820	0.5795	0.5339	0.5250	0.5551	0.5518	0.5518	0.3406
-0.4	0.3657	0.5580	0.5558	0.5060	0.5011	0.5302	0.5264	0.5251	0.3304
-0.3	0.3539	0.5327	0.5322	0.4804	0.4807	0.5065	0.5024	0.4998	0.3199
-0.2	0.3436	0.5095	0.5084	0.4554	0.4606	0.4835	0.4792	0.4772	0.3108
-0.1	0.3331	0.4867	0.4867	0.4304	0.4444	0.4621	0.4572	0.4556	0.2981
0.0	0.3216	0.4626	0.4631	0.4069	0.4270	0.4399	0.4349	0.4332	0.2865
0.1	0.3098	0.4423	0.4394	0.3830	0.4112	0.4190	0.4141	0.4126	0.2742
0.2	0.2981	0.4188	0.4194	0.3617	0.3926	0.3981	0.3930	0.3926	0.2626
0.3	0.2844	0.4007	0.3965	0.3396	0.3776	0.3786	0.3735	0.3736	0.2491
0.4	0.2708	0.3814	0.3768	0.3164	0.3634	0.3595	0.3539	0.3546	0.2353
0.5	0.2564	0.3622	0.3593	0.2962	0.3488	0.3416	0.3357	0.3344	0.2237
0.6	0.2410	0.3402	0.3402	0.2755	0.3328	0.3222	0.3162	0.3162	0.2089
0.7	0.2238	0.3200	0.3200	0.2576	0.3145	0.3030	0.2972	0.2948	0.1897
0.8	0.2066	0.2974	0.2976	0.2380	0.2942	0.2818	0.2756	0.2771	0.1718
0.9	0.1844	0.2709	0.2691	0.2169	0.2700	0.2567	0.2509	0.2516	0.1496
1.0	0.1623	0.2412	0.2410	0.1960	0.2396	0.2294	0.2217	0.2224	0.1320
Diff.	0.0361	0.1967	0.1957	0.1413	0.1611	0.1737	0.1685	0.1680	-

Table 13: Diff between \widehat{CLS} and oracle CLS under the QDA setting

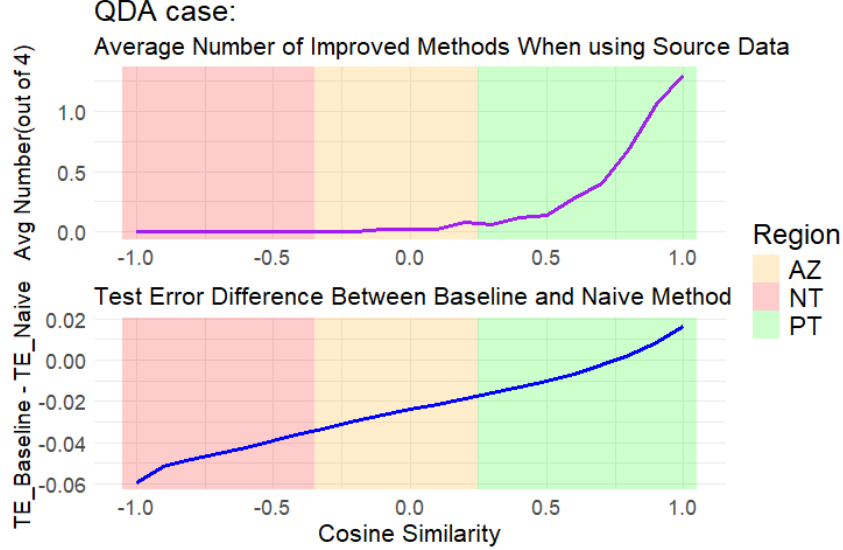


Figure 17: Transferability zones (positive, ambiguous, and negative) identified under the QDA model

For CLS estimation, we employ four regression models: linear regression, linear SVM, radial basis function (RBF) SVM, and XGBoost.

For the dataset similarity metric OTDD (Optimal Transport Dataset Distance), it is specifically designed for supervised classification tasks, and thus cannot be directly computed in regression settings due to the continuous nature of the labels.

Among the four transfer learning methods evaluated in Section 5.3 (Evaluation of Transferable Zones), both TrAdaBoost and Dynamic TrAdaBoost were originally developed for binary classification tasks and are therefore not applied in the regression experiments. To enable transfer learning in regression settings, we additionally incorporate the TrAdaBoost.R2 algorithm (Pardoe and Stone, 2010), which extends TrAdaBoost to handle regression problems.

B.3.1 Linear Regression Setting

Consider a binary classification problem where the features $\mathbf{x}_i \in \mathbb{R}^p$ (for sample index $i = 1, \dots, n_t$ for the target dataset and $i = 1, \dots, n_s$ for the source dataset) are independently and identically distributed (i.i.d.) as $\mathbf{x}_i \sim \mathcal{N}_p(0, \mathbf{I}_p)$, and the relationship between features and labels follows a linear model

$$y_i = \mathbb{I}[(\beta^\top \mathbf{x}_i + \xi_i) \geq 0],$$

where $\beta \in \mathbb{R}^p$ is the parameter vector, $\xi_i \sim \mathcal{N}(0, 1)$ is a random noise term, and $\mathbb{I}[\cdot]$ denotes the indicator function.

We consider two datasets: the target dataset, characterized by the parameter vector $\beta^{(t)}$, and the source dataset, characterized by the parameter vector $\beta^{(s)}$. We replace β in the above linear Probit model with $\beta^{(t)}$ and $\beta^{(s)}$ to generate the target and source datasets, respectively. The coefficient vector $\beta^{(t)}$ for the target data is drawn from $\mathcal{N}_p(\frac{1}{4}\mathbf{1}, \frac{1}{16}\mathbf{I}_p)$, where $\mathbf{1}$ denotes a p -dimensional vector of ones and \mathbf{I}_p denotes the $p \times p$ identity matrix. The vector $\beta^{(s)}$ is generated using the method described in Section B.1 to control the cosine similarity between $\beta^{(t)}$ and $\beta^{(s)}$. We set the feature dimension $p = 10$.

We consider two datasets: the target dataset, characterized by the parameter vector $\beta^{(t)}$, and the source dataset, characterized by the parameter vector $\beta^{(s)}$. We replace β mentioned above in the linear regression model with $\beta^{(t)}$, $\beta^{(s)}$ to generate the target and source dataset. The coefficient vector $\beta^{(t)}$ for the target data is drawn from $\mathcal{N}_p(\frac{1}{4}\mathbf{1}, \frac{1}{16}\mathbf{I}_p)$, where $\mathbf{1}$ denotes a p -dimensional vector of ones, and \mathbf{I}_p denotes the $p \times p$ identity matrix. The vector $\beta^{(s)}$ is generated using the method described in Section B.1 to control the cosine similarity between $\beta^{(t)}$ and $\beta^{(s)}$. We set the feature dimension $p = 10$.

The Oracle CLS is computed using $\beta^{(t)}$, $\beta^{(s)}$ based on the above data generation mechanism.

All results for this setting are presented in Table 14, Table 15, Figure 18, and Figure 19.

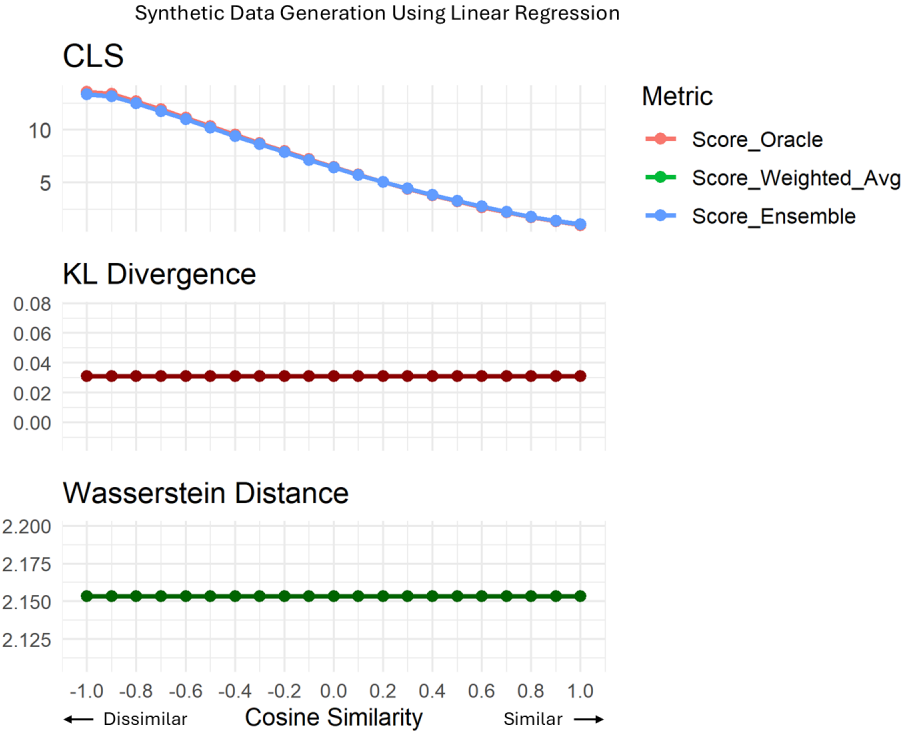


Figure 18: Comparison of CLS vs other similarity metrics under the Linear Regression Setting

Cosine Sim.	Score Oracle	Score Unw. Avg	Score Wtd. Avg	Score Ens.	KL Div.	Wass. Dist.
-1.0	13.5454	12.3923	13.3194	13.3200	0.0309	2.1533
-0.9	13.3761	12.2610	13.1404	13.1412	0.0309	2.1533
-0.8	12.6893	11.6569	12.4708	12.4719	0.0309	2.1533
-0.7	11.9252	10.9891	11.7301	11.7316	0.0309	2.1533
-0.6	11.1315	10.2725	10.9586	10.9585	0.0309	2.1533
-0.5	10.3283	9.5562	10.1788	10.1787	0.0309	2.1533
-0.4	9.5272	8.8366	9.4016	9.4018	0.0309	2.1533
-0.3	8.7357	8.1245	8.6327	8.6328	0.0309	2.1533
-0.2	7.9593	7.4421	7.8780	7.8780	0.0309	2.1533
-0.1	7.2021	6.7747	7.1413	7.1404	0.0309	2.1533
0.0	6.4677	6.1289	6.4255	6.4242	0.0309	2.1533
0.1	5.7592	5.5064	5.7349	5.7337	0.0309	2.1533
0.2	5.0792	4.9126	5.0719	5.0702	0.0309	2.1533
0.3	4.4304	4.3492	4.4389	4.4363	0.0309	2.1533
0.4	3.8152	3.8103	3.8387	3.8363	0.0309	2.1533
0.5	3.2362	3.3037	3.2770	3.2790	0.0309	2.1533
0.6	2.6960	2.8286	2.7459	2.7475	0.0309	2.1533
0.7	2.1979	2.3956	2.2516	2.2502	0.0309	2.1533
0.8	1.7456	1.9941	1.8056	1.8044	0.0309	2.1533
0.9	1.3446	1.6383	1.4087	1.4073	0.0309	2.1533
1.0	1.0041	1.3340	1.0711	1.0700	0.0309	2.1533
$ \rho_p $	0.9960	0.9957	0.9962	0.9962	0.0000	0.0000
$ \rho_s $	1.0000	1.0000	1.0000	1.0000	0.0000	0.0000

Table 14: Comparison of similarity metrics across varying cosine similarity values under the Linear Regression setting

Cos. Sim.	Lin. Repr.	SVM Linear	SVM Radial	Xgb Tree	Score Unw. Avg	Score Wtd. Avg	Score Ens.	Score Oracle
-1.0	13.3158	13.3412	11.3723	11.5400	12.3923	13.3194	13.3200	13.5454
-0.9	13.1410	13.1610	11.2278	11.5143	12.2610	13.1404	13.1412	13.3761
-0.8	12.4727	12.4880	10.6712	10.9955	11.6569	12.4708	12.4719	12.6893
-0.7	11.7306	11.7449	10.0514	10.4297	10.9891	11.7301	11.7316	11.9252
-0.6	10.9600	10.9719	9.4090	9.7489	10.2725	10.9586	10.9585	11.1315
-0.5	10.1804	10.1949	8.7577	9.0920	9.5562	10.1788	10.1787	10.3283
-0.4	9.4025	9.4183	8.1098	8.4158	8.8366	9.4016	9.4018	9.5272
-0.3	8.6337	8.6512	7.4722	7.7410	8.1245	8.6327	8.6328	8.7357
-0.2	7.8790	7.8973	6.8515	7.1404	7.4421	7.8780	7.8780	7.9593
-0.1	7.1426	7.1609	6.2478	6.5476	6.7747	7.1413	7.1404	7.2021
0.0	6.4278	6.4463	5.6639	5.9774	6.1289	6.4255	6.4242	6.4677
0.1	5.7376	5.7557	5.1029	5.4295	5.5064	5.7349	5.7337	5.7592
0.2	5.0744	5.0929	4.5673	4.9157	4.9126	5.0719	5.0702	5.0792
0.3	4.4407	4.4593	4.0594	4.4375	4.3492	4.4389	4.4363	4.4304
0.4	3.8390	3.8572	3.5828	3.9621	3.8103	3.8387	3.8363	3.8152
0.5	3.2717	3.2894	3.1378	3.5159	3.3037	3.2770	3.2790	3.2362
0.6	2.7413	2.7598	2.7257	3.0876	2.8286	2.7459	2.7475	2.6960
0.7	2.2509	2.2691	2.3483	2.7141	2.3956	2.2516	2.2502	2.1979
0.8	1.8040	1.8212	2.0087	2.3426	1.9941	1.8056	1.8044	1.7456
0.9	1.4060	1.4237	1.7116	2.0117	1.6383	1.4087	1.4073	1.3446
1.0	1.0658	1.0892	1.4730	1.7081	1.3340	1.0711	1.0700	1.0041
Diff.	0.0942	0.0918	0.962	0.8356	0.4871	0.0957	0.0954	-

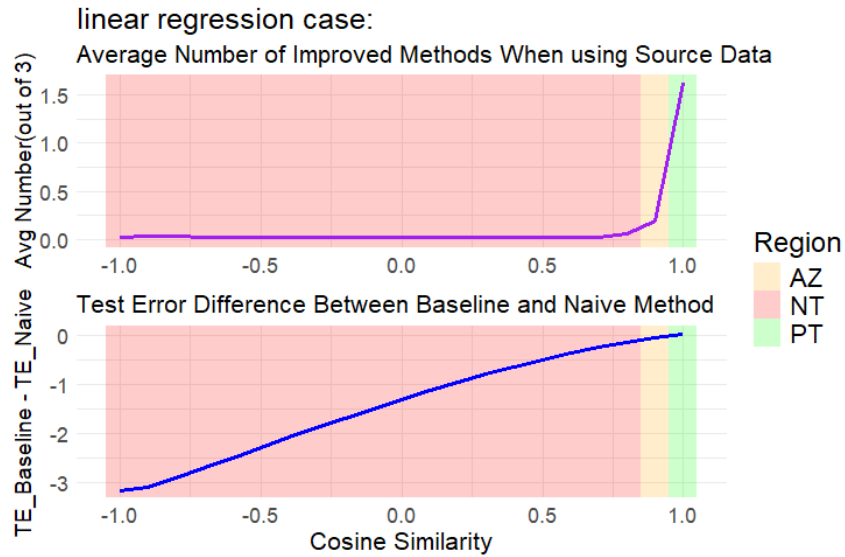
Table 15: Diff between \widehat{CLS} and oracle CLS under the Linear Regression setting

Figure 19: Transferability zones (positive, ambiguous, and negative) identified under the linear regression model

B.3.2 Non-linear Regression Setting

Consider a regression problem where the features $\mathbf{x}_i \in \mathbb{R}^p$ (for sample index $i = 1, \dots, n_t$ for the target dataset and $i = 1, \dots, n_s$ for the source dataset) are independently and identically distributed (i.i.d.) as $\mathbf{x}_i \sim \mathcal{N}_p(0, I_p)$. We set the feature dimension to $p = 10$. Among these ten features, only the first five are used to generate the response variable y_i through the following nonlinear function:

$$y_i = \beta_1 \sin(x_{i1}) + \beta_2 x_{i2}^2 + \beta_3 x_{i3} x_{i4} + \beta_4 \exp(x_{i5}) + \epsilon_i,$$

where $\beta = (\beta_1, \beta_2, \beta_3, \beta_4)$ is the parameter vector, $\epsilon_i \sim \mathcal{N}(0, 1)$ denotes Gaussian noise, and x_{ij} represents the j -th feature of the i -th sample.

We consider two datasets: the target dataset, characterized by the parameter vector $\beta^{(t)}$, and the source dataset, characterized by the parameter vector $\beta^{(s)}$. We replace β in the above nonlinear regression model with $\beta^{(t)}$ and $\beta^{(s)}$ to generate the target and source datasets, respectively. The coefficient vector $\beta^{(t)}$ for the target data is drawn from $\mathcal{N}_4(\frac{1}{4}\mathbf{1}_4, \frac{1}{16}\mathbf{I}_4)$, where $\mathbf{1}_4$ denotes a four-dimensional vector of ones and \mathbf{I}_4 denotes the 4×4 identity matrix. The vector $\beta^{(s)}$ is generated using the method described in Section B.1 to control the cosine similarity between $\beta^{(t)}$ and $\beta^{(s)}$.

The Oracle CLS is computed using $\beta^{(t)}, \beta^{(s)}$ based on the above data generation mechanism.

All results for this setting are presented in Table 16, Table 17, Figure 20, and Figure 21.

From Figure 20, we observe that the estimated CLS values (both the weighted-average and ensemble schemes) do not closely approximate the oracle. This observation can be explained by the results in Table 17, where the *Diff.* values of all four single models are relatively high compared with the optimal model (QDA). This indicates that the selected models—linear regression, linear SVM, radial SVM, and XGBoost—do not fit the data well. Nevertheless, several consistent patterns can still be identified: (1) in this nonlinear setting, nonlinear models (radial SVM and XGBoost) outperform linear ones; and (2) the ensemble estimate (Ens.) achieves better performance than both the weighted-average (Wtd. Avg.) and unweighted-average (Unw. Avg.) estimates.

Moreover, from Figure 20, we find that the estimated CLS values do not decrease monotonically as the cosine similarity increases. This phenomenon can be further interpreted using the results in Figure 21. As shown in the bottom panel, for the naive transfer method, the test error difference between the baseline and the naive method does not vary monotonically with cosine similarity: when the cosine similarity is below -0.8 , the difference decreases monotonically, whereas when the cosine similarity exceeds -0.8 , the difference begins to increase. This indicates that, under this setting, data similarity (or transferability) does not change monotonically with cosine similarity but instead follows the same trend observed in the bottom panel of Figure 21. Importantly, the estimated CLS in Figure 20 exhibits a consistent trend, further demonstrating that our CLS effectively captures the underlying data similarity (transferability).

B.4 Synthetic Data Generation for Multi-class Classification

For multi-class classification, we design a four-class task in which samples are projected onto two orthogonal directions and assigned to quadrants based on the signs of the projections, with Gaussian noise added for perturbation.

For CLS estimation, we employ four models for multi-class classification: multinomial logistic regression, linear SVM, radial basis function (RBF) SVM, and XGBoost.

Among the four transfer learning methods evaluated in Section 5.3 (Evaluation of Transferable Zones), both TrAdaBoost and Dynamic TrAdaBoost are originally developed for binary classification, and therefore are not applied in the multi-class classification experiments.

B.4.1 4-class Classification Setting

We consider a four-class classification problem in which the feature vectors $\mathbf{x}_i \in \mathbb{R}^p$ (for sample index $i = 1, \dots, n_t$ for the target dataset and $i = 1, \dots, n_s$ for the source dataset) are independently and identically distributed (i.i.d.) as $\mathbf{x}_i \sim \mathcal{N}_p(\mathbf{0}, I_p)$, with the feature dimension set to $p = 10$. We generate the data using two parameter vectors $\beta_1, \beta_2 \in \mathbb{R}^p$, which are constructed to be orthogonal, i.e., $\beta_1 \perp \beta_2$.

Given the first coefficient vector β_1 , the second coefficient vector β_2 is constructed such that $\beta_1^\top \beta_2 = 0$ and $\|\beta_2\| = \|\beta_1\|$, using the Gram–Schmidt orthogonalization procedure.

Given β_1 and β_2 , the class label for each sample \mathbf{x}_i is determined by the signs of its projections onto the two parameter vectors:

$$\zeta_1 = \mathbf{x}_i^\top \beta_1 + \epsilon_1, \quad \zeta_2 = \mathbf{x}_i^\top \beta_2 + \epsilon_2,$$

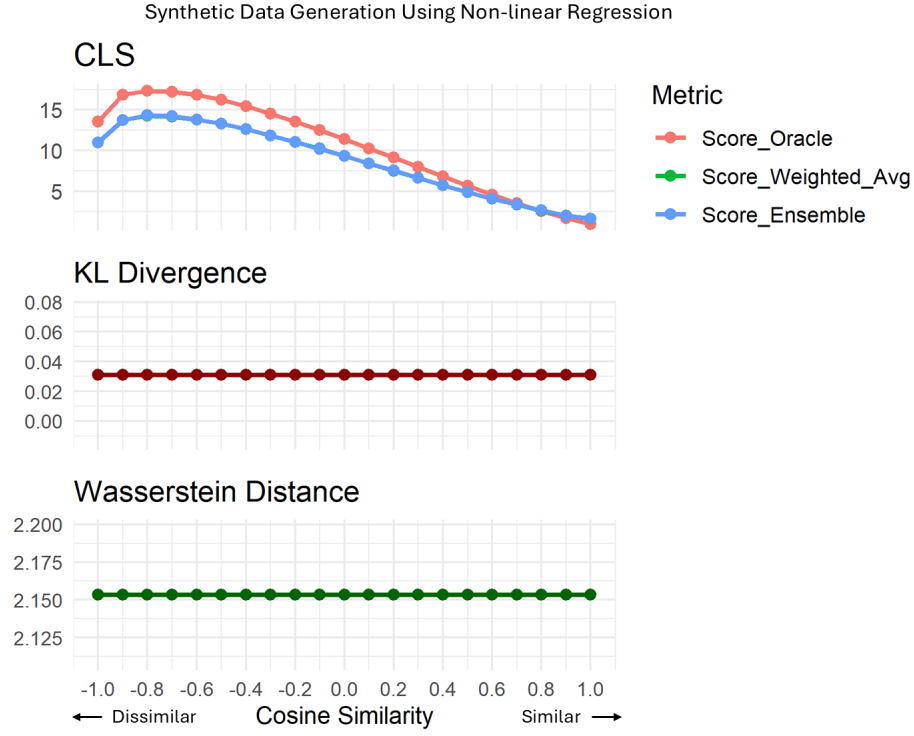


Figure 20: Comparison of CLS vs other similarity metrics under the Non-linear Regression Setting

Cosine Sim.	Score Oracle	Score Unw. Avg	Score Wtd. Avg	Score Ens.	KL Div.	Wass. Dist.
-1.0	13.5836	10.6483	11.0070	11.0179	0.0309	2.1533
-0.9	16.8592	13.0626	13.7364	13.7297	0.0309	2.1533
-0.8	17.3334	13.3941	14.2699	14.3309	0.0309	2.1533
-0.7	17.2469	13.3371	14.1895	14.2496	0.0309	2.1533
-0.6	16.8425	13.0261	13.7770	13.8052	0.0309	2.1533
-0.5	16.2236	12.5714	13.3188	13.3460	0.0309	2.1533
-0.4	15.4488	12.0044	12.6303	12.6177	0.0309	2.1533
-0.3	14.5565	11.3369	11.8536	11.8354	0.0309	2.1533
-0.2	13.5747	10.6034	11.0730	11.0544	0.0309	2.1533
-0.1	12.5252	9.8270	10.2380	10.2124	0.0309	2.1533
0.0	11.4261	9.0225	9.3352	9.3231	0.0309	2.1533
0.1	10.2929	8.1868	8.4433	8.4484	0.0309	2.1533
0.2	9.1399	7.3408	7.5453	7.5631	0.0309	2.1533
0.3	7.9802	6.4925	6.6359	6.6603	0.0309	2.1533
0.4	6.8270	5.6589	5.7340	5.7591	0.0309	2.1533
0.5	5.6936	4.8478	4.8925	4.9156	0.0309	2.1533
0.6	4.5943	4.0680	4.0887	4.1099	0.0309	2.1533
0.7	3.5459	3.3369	3.3421	3.3598	0.0309	2.1533
0.8	2.5693	2.6825	2.6594	2.6712	0.0309	2.1533
0.9	1.6960	2.1301	2.0464	2.0453	0.0309	2.1533
1.0	1.0041	1.8465	1.6325	1.6251	0.0309	2.1533
$ \rho_p $	0.9594	0.9601	0.9585	0.9587	0.0000	0.0000
$ \rho_s $	0.9597	0.9597	0.9455	0.9455	0.0000	0.0000

Table 16: Comparison of similarity metrics across varying cosine similarity values under the Non-linear Regression setting

Cos. Sim.	Non-Lin. Repr.	Lin. Repr.	SVM Linear	SVM Radial	Xgb Tree	Score Unw. Avg	Score Wtd. Avg	Score Ens.	Score Oracle
-1.0	13.0749	10.4454	9.7830	10.7185	11.6464	10.6483	11.0070	11.0179	13.5836
-0.9	16.1493	12.7993	11.8219	13.1570	14.4472	13.0626	13.7364	13.7297	16.8592
-0.8	16.5904	13.1358	12.0997	13.5097	14.8310	13.3941	14.2699	14.3309	17.3334
-0.7	16.5046	13.0654	12.0281	13.4448	14.8102	13.3371	14.1895	14.2496	17.2469
-0.6	16.1198	12.7642	11.7640	13.1423	14.4340	13.0261	13.7770	13.8052	16.8425
-0.5	15.5333	12.3078	11.3560	12.6808	13.9409	12.5714	13.3188	13.3460	16.2236
-0.4	14.8000	11.7392	10.8499	12.1044	13.3240	12.0044	12.6303	12.6177	15.4488
-0.3	13.9560	11.0870	10.2572	11.4402	12.5632	11.3369	11.8536	11.8354	14.5565
-0.2	13.0274	10.3721	9.6234	10.7090	11.7090	10.6034	11.0730	11.0544	13.5747
-0.1	12.0349	9.6111	8.9493	9.9251	10.8226	9.8270	10.2380	10.2124	12.5252
0.0	10.9951	8.8177	8.2393	9.1053	9.9275	9.0225	9.3352	9.3231	11.4261
0.1	9.9228	8.0042	7.5131	8.2623	8.9675	8.1868	8.4433	8.4484	10.2929
0.2	8.8312	7.1817	6.7636	7.4065	8.0114	7.3408	7.5453	7.5631	9.1399
0.3	7.7326	6.3610	6.0097	6.5447	7.0544	6.4925	6.6359	6.6603	7.9802
0.4	6.6392	5.5530	5.2703	5.6858	6.1264	5.6589	5.7340	5.7591	6.8270
0.5	5.5634	4.7690	4.5433	4.8444	5.2346	4.8478	4.8925	4.9156	5.6936
0.6	4.5185	4.0222	3.8412	4.0277	4.3808	4.0680	4.0887	4.1099	4.5943
0.7	3.5199	3.3283	3.1841	3.2538	3.5816	3.3369	3.3421	3.3598	3.5459
0.8	2.5867	2.7095	2.6115	2.5602	2.8486	2.6825	2.6594	2.6712	2.5693
0.9	1.7472	2.2050	2.1675	1.9705	2.1772	2.1301	2.0464	2.0453	1.6960
1.0	1.0627	2.0243	2.0594	1.6243	1.6780	1.8465	1.6325	1.6251	1.0041
Diff.	0.3956	2.3809	2.9222	2.1255	1.3982	2.2056	1.8406	1.8299	-

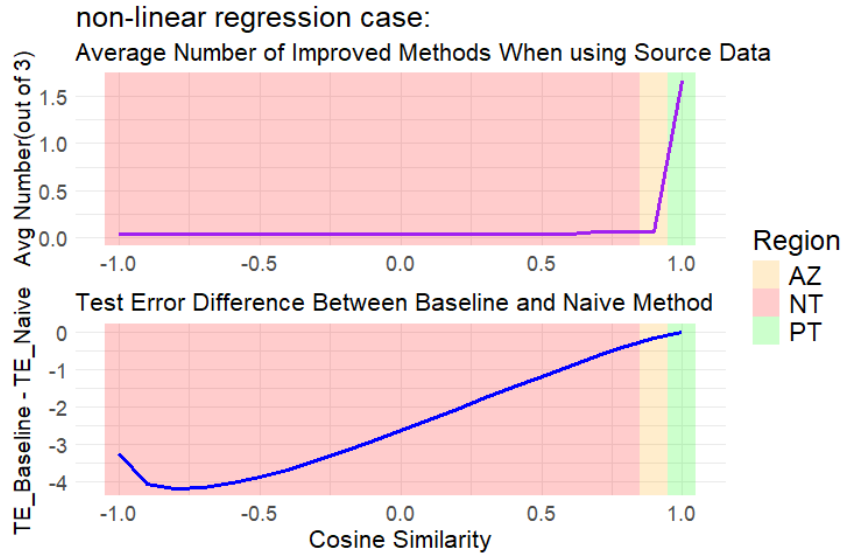
Table 17: Diff between \overline{CLS} and oracle CLS under the Non-linear Regression setting

Figure 21: Transferability zones (positive, ambiguous, and negative) identified under the non-linear regression model

where $\epsilon_1, \epsilon_2 \sim \mathcal{N}(0, \sigma^2)$ are independent Gaussian noise terms that introduce soft decision boundaries and we set the noise level $\sigma = 0.3$. The resulting class label y_i is assigned according to the quadrant in the projection space:

$$y_i = \begin{cases} 1, & \text{if } \zeta_1 < 0 \text{ and } \zeta_2 < 0, \\ 2, & \text{if } \zeta_1 < 0 \text{ and } \zeta_2 \geq 0, \\ 3, & \text{if } \zeta_1 \geq 0 \text{ and } \zeta_2 < 0, \\ 4, & \text{if } \zeta_1 \geq 0 \text{ and } \zeta_2 \geq 0. \end{cases}$$

This construction yields a synthetic dataset with four linearly separable classes in the (ζ_1, ζ_2) plane, while the Gaussian noise (ϵ_1, ϵ_2) controls the degree of boundary smoothness.

We consider two datasets: the target dataset characterized by the pair $(\beta_1^{(t)}, \beta_2^{(t)})$ and the source dataset characterized by the pair $(\beta_1^{(s)}, \beta_2^{(s)})$. We replace (β_1, β_2) mentioned above with $(\beta_1^{(t)}, \beta_2^{(t)})$, $(\beta_1^{(s)}, \beta_2^{(s)})$ to generate the target and source dataset separately.

The coefficient vector $\beta_1^{(t)}$ for the target data is drawn from $\mathcal{N}_p(\frac{1}{4}\mathbf{1}, \frac{1}{16}\mathbf{I}_p)$, where $\mathbf{1}$ denotes a p -dimensional vector of ones, and \mathbf{I}_p denotes the $p \times p$ identity matrix. The coefficient vector $\beta_2^{(t)}$ is constructed such that $\beta_1^{(t)\top} \beta_2^{(t)} = 0$ and $\|\beta_2^{(t)}\| = \|\beta_1^{(t)}\|$ using the Gram–Schmidt orthogonalization procedure.

We control the similarity between the datasets by adjusting the cosine similarity between $\beta_1^{(t)}$ and $\beta_1^{(s)}$ using the procedure described in Section B.1, and $\beta_2^{(s)}$ is constructed such that $\beta_1^{(s)\top} \beta_2^{(s)} = 0$ and $\|\beta_2^{(s)}\| = \|\beta_1^{(s)}\|$ using the Gram–Schmidt orthogonalization procedure.

The Oracle CLS is then computed using $(\beta_1^{(t)}, \beta_2^{(t)})$ and $(\beta_1^{(s)}, \beta_2^{(s)})$ based on the above data generation mechanism.

All results for this setting are presented in Table 18, Table 19, Figure 22, and Figure 23.

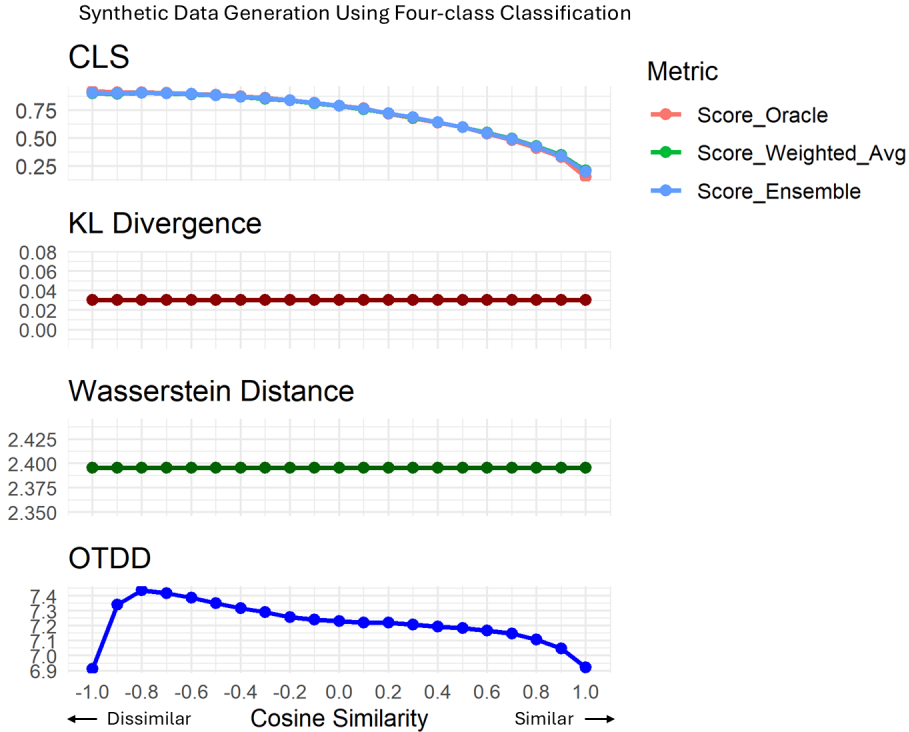


Figure 22: Comparison of CLS vs other similarity metrics under the 4-Class Classification Setting

C ADDITIONAL MATERIAL FOR SECTION 6

In addition to the *eICU Mortality Prediction* and *Canine Image Classification* experiments described in the main text, we also conducted a *Handwritten Digit Recognition* experiment using real-world data.

Cosine Sim.	Score Oracle	Score Unw. Avg	Score Wtd. Avg	Score Ens.	KL Div.	Wass. Dist.	OTDD
-1.0	0.9257	0.8808	0.9016	0.9076	0.0304	2.3958	6.9123
-0.9	0.9097	0.8841	0.8974	0.9008	0.0304	2.3958	7.3415
-0.8	0.9106	0.8916	0.9039	0.9050	0.0304	2.3958	7.4359
-0.7	0.9073	0.8893	0.9007	0.9020	0.0304	2.3958	7.4181
-0.6	0.8990	0.8827	0.8928	0.8955	0.0304	2.3958	7.3883
-0.5	0.8899	0.8737	0.8832	0.8852	0.0304	2.3958	7.3518
-0.4	0.8750	0.8615	0.8698	0.8712	0.0304	2.3958	7.3187
-0.3	0.8592	0.8458	0.8540	0.8554	0.0304	2.3958	7.2889
-0.2	0.8399	0.8292	0.8368	0.8384	0.0304	2.3958	7.2585
-0.1	0.8140	0.8070	0.8130	0.8150	0.0304	2.3958	7.2418
0.0	0.7880	0.7833	0.7897	0.7913	0.0304	2.3958	7.2310
0.1	0.7660	0.7526	0.7585	0.7608	0.0304	2.3958	7.2201
0.2	0.7181	0.7180	0.7217	0.7232	0.0304	2.3958	7.2198
0.3	0.6776	0.6821	0.6842	0.6860	0.0304	2.3958	7.2073
0.4	0.6368	0.6432	0.6432	0.6438	0.0304	2.3958	7.1947
0.5	0.5964	0.5991	0.5966	0.5968	0.0304	2.3958	7.1828
0.6	0.5409	0.5517	0.5463	0.5443	0.0304	2.3958	7.1689
0.7	0.4827	0.5034	0.4947	0.4923	0.0304	2.3958	7.1468
0.8	0.4079	0.4404	0.4259	0.4222	0.0304	2.3958	7.1090
0.9	0.3283	0.3683	0.3466	0.3406	0.0304	2.3958	7.0496
1.0	0.1518	0.2543	0.2104	0.1991	0.0304	2.3958	6.9209
$ \rho_p $	0.9292	0.9334	0.9314	0.9303	0.0000	0.0000	0.5741
$ \rho_s $	0.9987	0.9831	0.9935	0.9961	0.0000	0.0000	0.7143

Table 18: Comparison of similarity metrics across varying cosine similarity values under the 4-class Classification setting

Cos. Sim.	MLR	SVM Linear	SVM Radial	Xgb Tree	Score Unw. Avg	Score Wtd. Avg	Score Ens.	Score Oracle
-1.0	0.9072	0.9003	0.8802	0.8356	0.8808	0.9016	0.9076	0.9257
-0.9	0.9012	0.8976	0.8850	0.8526	0.8841	0.8974	0.9008	0.9097
-0.8	0.9062	0.9040	0.8938	0.8623	0.8916	0.9039	0.9050	0.9106
-0.7	0.9028	0.9016	0.8929	0.8600	0.8893	0.9007	0.9020	0.9073
-0.6	0.8950	0.8942	0.8865	0.8550	0.8827	0.8928	0.8955	0.8990
-0.5	0.8862	0.8834	0.8769	0.8482	0.8737	0.8832	0.8852	0.8899
-0.4	0.8713	0.8722	0.8638	0.8386	0.8615	0.8698	0.8712	0.8750
-0.3	0.8561	0.8543	0.8478	0.8251	0.8458	0.8540	0.8554	0.8592
-0.2	0.8392	0.8373	0.8288	0.8114	0.8292	0.8368	0.8384	0.8399
-0.1	0.8155	0.8121	0.8075	0.7931	0.8070	0.8130	0.8150	0.8140
0.0	0.7914	0.7889	0.7849	0.7680	0.7833	0.7897	0.7913	0.7880
0.1	0.7608	0.7574	0.7532	0.7390	0.7526	0.7585	0.7608	0.7660
0.2	0.7246	0.7206	0.7196	0.7073	0.7180	0.7217	0.7232	0.7181
0.3	0.6868	0.6826	0.6815	0.6778	0.6821	0.6842	0.6860	0.6776
0.4	0.6442	0.6424	0.6440	0.6423	0.6432	0.6432	0.6438	0.6368
0.5	0.5954	0.5954	0.5995	0.6062	0.5991	0.5966	0.5968	0.5964
0.6	0.5434	0.5449	0.5538	0.5648	0.5517	0.5463	0.5443	0.5409
0.7	0.4907	0.4944	0.5034	0.5251	0.5034	0.4947	0.4923	0.4827
0.8	0.4219	0.4242	0.4415	0.4741	0.4404	0.4259	0.4222	0.4079
0.9	0.3402	0.3469	0.3700	0.4161	0.3683	0.3466	0.3406	0.3283
1.0	0.1996	0.2102	0.2616	0.3458	0.2543	0.2104	0.1991	0.1518
Diff.	0.1694	0.2057	0.4173	0.9358	0.4229	0.2154	0.1725	-

Table 19: Diff between \widehat{CLS} and oracle CLS under the 4-Class Classification Setting

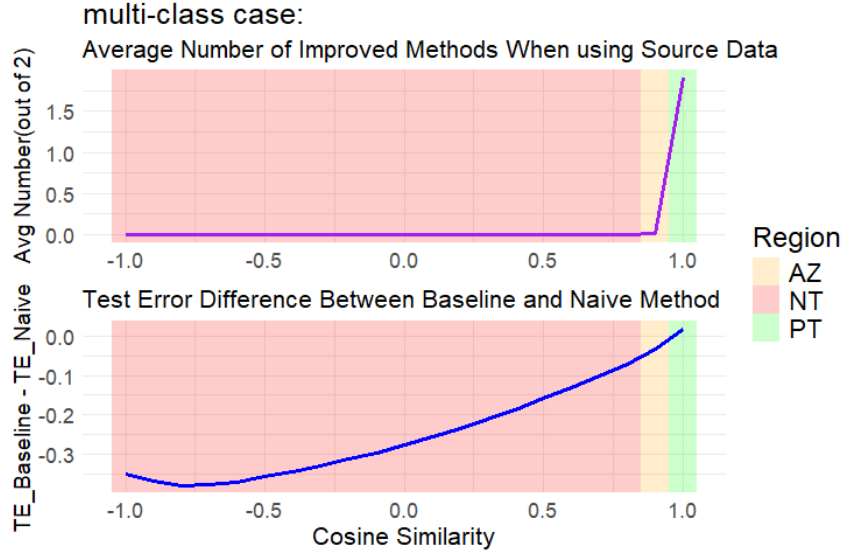


Figure 23: Transferability zones (positive, ambiguous, and negative) identified under the 4-class classification model

All experiments were performed on the High Performance Computing (HPC) cluster, equipped with one NVIDIA Tesla P100 GPU (16GB), 4 CPU cores, and 32GB of system memory. Each experiment was repeated 10 times, and the reported results represent the average across all runs.

Our code and data will be released publicly upon acceptance.

C.1 eICU Mortality Prediction

More details about this experiment are described here.

We study ICU mortality prediction using the eICU Collaborative Research Database (Pollard et al., 2018), a multi-center dataset containing de-identified health records from U.S. hospitals between 2014 and 2015. To predict the post-ICU survival status of patients, we constructed a feature set that integrates multiple aspects of patient care. The features include demographics and admission information (age, gender, ethnicity, height, weight, admission type, and ICU type), hospital-level descriptors (hospital identifier, bed capacity category, region, and teaching status), acute physiological variables from the APACHE APS system (vital signs, laboratory values, Glasgow Coma Scale components, and indicators of organ support such as intubation, ventilation, dialysis, and urine output), as well as chronic health conditions and comorbidities (diabetes, cirrhosis, metastatic cancer, immunosuppression, elective surgery status, and others). After removing records with missing data, we calculated the post-ICU mortality rate for each hospital. To balance the outcome distribution, we undersampled hospital data so that the number of survivors and non-survivors was equal.

Our target task is to predict post-ICU survival status in teaching hospitals. We designated the hospital with the highest mortality rate (9.47%, with $n_{\text{post-ICU alive}} = 43$) as the target dataset. Among the remaining hospitals, those with at least 50 post-ICU survivors were used as source datasets, yielding a total of 11 source hospitals.

We first evaluated the similarity between the target dataset and each source dataset using the ensemble CLS. The base models for the ensemble (logistic regression, linear SVM, radial SVM, and XGBoost) were consistent with those used in the numerical analysis section. For the target dataset, we then estimated the 5-fold cross-validation error and corresponding standard error using the ensemble model. Based on the error estimates, each source dataset was mapped to a transferability zone.

To verify whether these source datasets indeed yielded beneficial transfer, we conducted additional experiments following the Adaptive Robust Transfer Learning (ART) framework. For the target dataset (43 survivors and 43 non-survivors), we randomly sampled 30 survivors and 30 non-survivors as training data, with the remaining cases held out as test data. Using Random Forests, AdaBoost, and neural networks as candidate base models, we found that Random Forests consistently achieved the best baseline performance on the target dataset, with an average test error of 0.4077. We therefore adopted Random Forests as the base classifier for all subsequent transfer learning methods.

Table 20: Relative error reduction on USPS when using transfer learning.

Source Dataset	Relative Error Reduction	Zone
EMNIST/Digits	+0.344	PT
MNIST	+0.316	PT

C.2 Canine Image Classification

More details about this experiment are described here.

Our target dataset is the Roboflow Dogs vs Wolves dataset, which contains 194 dog images and 412 wolf images. The relatively small size and class imbalance make this dataset difficult to classify accurately. As source datasets, we considered: (i) Kaggle Dogs vs Wolves (1,000 dogs and 1,000 wolves), which is more balanced and substantially larger; (ii) Kaggle Cats vs Dogs (a random sample of 1,000 cats and 1,000 dogs), which shares one class with the target task but introduces a distinct source species; and (iii) Kaggle Horses vs Camels (200 horses and 200 camels), which has a similar binary structure but with entirely different categories. These source datasets provide different levels of semantic and distributional similarity relative to the target task.

We employed the Encoder–Head CLS introduced in Algorithm 3, this time using ResNet-18 as the backbone encoder. Because ResNet-18 has substantially more parameters than LeNet-5, we initialized the model with ImageNet-pretrained weights to ensure stable convergence. As before, a shared encoder was trained jointly on the target and source datasets, followed by domain-specific heads for cross-domain evaluation.

For empirical validation, we used the 5-fold cross-validation to estimate the test errors.

C.3 Handwritten Digit Recognition

Handwritten digit recognition is a classic benchmark for evaluating model generalization and transfer learning. Unlike clinical data, digit datasets provide a controlled setting where domain shifts primarily arise from differences in writing style, resolution, and dataset size, making them an ideal testbed for validating our similarity-based framework (Zhong and Tandon, 2023, 2024b,a, 2025; Zhang et al., 2024). We designate USPS as the target dataset because it is smaller in sample size and more challenging to classify relative to common source datasets (e.g., MNIST, EMNIST/Digits). The increased difficulty stems from fewer training examples and lower image resolution (16×16), which together make USPS a stringent target domain. By testing whether transfer learning from large, diverse datasets such as MNIST and EMNIST/Digits improves USPS performance, we can evaluate whether our proposed CLS-based zone predictions align with empirical transfer outcomes in a well-studied vision setting.

The target dataset is USPS (grayscale 16×16 , digits 0–9). The source datasets are MNIST and EMNIST/Digits (both grayscale 28×28). These source datasets provide substantially larger training corpora and stylistic diversity, creating a realistic distribution shift scenario for transfer to the smaller, harder USPS target.

We employ the Encoder–Head CLS introduced in Algorithm 3. Concretely, a shared LeNet-5 encoder is trained jointly on the target and a source dataset; then two domain-specific heads are trained to support cross-domain evaluation. We compute the encoder–head CLS estimate $\widehat{\text{CLS}}_{\text{Enc-Head}}$ and compare it against the baseline error on the target dataset e_0 and its standard error following the zone-mapping rule. Importantly, we repeat the entire estimation procedure 10 times and report the mean and standard error across runs; based on these aggregated estimates (rather than per-run decisions), both MNIST and EMNIST/Digits are placed in the Positive Transfer Zone.

Using LeNet-5 trained only on USPS, the 5-fold cross-validation error is 0.0244. With transfer learning—pretraining on an source dataset and then fine-tuning on USPS—the USPS 5-fold CV performance improves, achieving a relative error reduction of +0.344 with EMNIST/Digits and +0.316 with MNIST (Table 20). These results (averaged over 10 repetitions) validate the zone predictions derived from $\widehat{\text{CLS}}_{\text{Enc-Head}}$, confirming that both source datasets lie in the Positive Transfer Zone and yield tangible performance gains on the USPS target.